applied sciences

MDPI

Review

Connections between Metallic Nanoparticles and Chlorin e6—An Overview of Physicochemical and Biological Properties and Prospective Medical Applications

Tomasz Koczorowski [1,*], Arleta Glowacka-Sobotta [2], Maciej Michalak [3], Dariusz T. Mlynarczyk [1], Emre Güzel [4,5], Tomasz Goslinski [1] and Lukasz Sobotta [3]

[1] Chair and Department of Chemical Technology of Drugs, Poznan University of Medical Sciences, Grunwaldzka 6, 60-780 Poznan, Poland
[2] Chair and Department of Orthodontics and Temporomandibular Disorders, Poznan University of Medical Sciences, Bukowska 70, 60-812 Poznan, Poland
[3] Chair and Department of Inorganic and Analytical Chemistry, Poznan University of Medical Sciences, Rokietnicka 3, 60-806 Poznan, Poland
[4] Department of Engineering Fundamental Sciences, Sakarya University of Applied Sciences, 54050 Sakarya, Türkiye
[5] Biomedical Technologies Application and Research Center (BIYOTAM), Sakarya University of Applied Sciences, 54050 Sakarya, Türkiye
* Correspondence: tkoczorowski@ump.edu.pl

Abstract: Photodynamic therapy is a non-invasive method of treatment for both neoplastic diseases and miscellaneous non-cancerous illnesses. It is complementary and, in some way, counter to various traditional treatment techniques, including chemotherapy, radiotherapy, and surgery. To date, various types of nanoparticles and compounds, including those belonging to the porphyrinoid group, have been researched in terms of future applications in technology and medicine. Among them, chlorins and their conjugates, combined with metallic nanoparticles, deserve special attention due to their enhanced photodynamic activity and the accompanied synergic photothermal effect. Many hybrid nanosystems reveal increased cellular uptake and improved stability and, therefore, can be applied in enhanced MRI imaging, as well as in targeting therapy. This review is focused on conjugates of metallic nanoparticles and chlorins, having in mind prospective applications as photosensitizers in multimodal neoplastic therapy, as well as tumor diagnosis.

Keywords: metallic nanoparticles; chlorins; photosensitizers; conjugates; photodynamic therapy

check for updates

Citation: Koczorowski, T.; Glowacka-Sobotta, A.; Michalak, M.; Mlynarczyk, D.T.; Güzel, E.; Goslinski, T.; Sobotta, L. Connections between Metallic Nanoparticles and Chlorin e6—An Overview of Physicochemical and Biological Properties and Prospective Medical Applications. *Appl. Sci.* **2023**, *13*, 3933. https://doi.org/10.3390/app13063933

Academic Editor: Giuliana Muzio

Received: 14 February 2023
Revised: 12 March 2023
Accepted: 15 March 2023
Published: 20 March 2023

Copyright: © 2023 by the authors. Licensee MDPI, Basel, Switzerland. This article is an open access article distributed under the terms and conditions of the Creative Commons Attribution (CC BY) license (https://creativecommons.org/licenses/by/4.0/).

1. Introduction

Chlorins, which are β,β-reduced porphyrins, are macrocyclic molecules resembling porphyrins, which occur naturally and constitute the main ingredients of chlorophylls. A reduced double bond in one of the four pyrrole macrocycle rings distinguishes them from porphyrins (Figure 1). Chlorin is the core chromophore of chlorophyll, a macrocycle of dihydroporphyrin containing one pyrrole ring and three pyrrole rings. They can be formed via prototropic tautomerization in suitable tetrapyrroles where the structural properties do not inhibit tautomerization. Due to its extraordinary photophysical properties, several new chlorins have been isolated from natural sources, such as marine microbes. In addition, several new synthetic analogs have been prepared as a result of the diligent work of chemists to explore structure–function relationships [1,2].

Chlorins, unlike porphyrins, exhibit intense absorption in both the blue and red regions, which can be attributed to their relatively lower symmetry. They exhibit characteristic optical features, which are altered from those of porphyrins, such as fluorescence, as well as a weaker Soret band and red-shifted, intensified Q-bands. These spectral properties are considered ideal for photosynthetic functions. In the spectra of chlorins, a strong absorption

band appears in the violet–blue region (~380–450 nm, known as the B band or Soret band) and in the red region (~600–700 nm, known as the Q band). The absorption of light in both regions produces a green color typical of chlorin, which can be observed in solution or thin films (for example, a leaf) upon illumination with white light [1]. The absorption properties of chlorins can be altered by peripheral substituents and metal ions chelated in the center of the macrocycle. The solubility of most chlorins in aqueous solutions is poor due to their strongly hydrophobic nature [2].

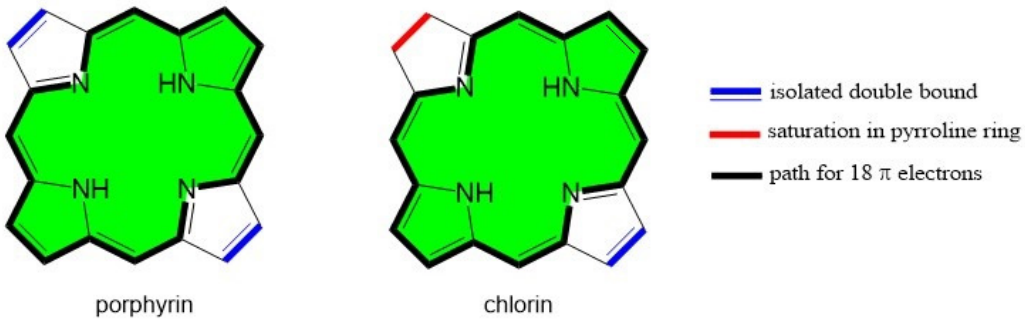


Figure 1. Differences and aromatic paths of chlorin and porphyrin.

Chlorins with NIR fluorescence emission have been applied in many disciplines of medicine, ranging from photodynamic therapy (PDT) to diagnostics, including flow cytometry and optical imaging [2]. PDT involves the localized application of the photosensitizer (PS) accompanied by its illumination in the tissue with a light beam of a specific wavelength. The light beam of required intensity should be absorbed by PS previously supplied to the treated tissue. Absorption of the light's quantum energy by PS molecules triggers a photodynamic reaction, which results in the generation of singlet oxygen and other reactive oxygen species (ROS) [3,4]. Since ROS are highly cytotoxic entities, this phenomenon has been applied to treatments of various tumorous tissues [4]. The ROS species also reveal an antimicrobial solid effect, which can be used against antibiotic-resistant microbes in the form of so-called photodynamic antimicrobial chemotherapy (PACT) [5–7].

In recent years, one of the most commonly used chlorins has been chlorin e6 (Ce6) (Figure 2). Other studies on novel chlorin-based PSs are ongoing. Chemical modifications of chlorin gave access to modified macrocycles of improved physicochemical properties, including higher water solubilities and more efficient singlet oxygen-generation abilities. Many modified chlorins reveal light absorption in the so-called phototherapeutic window, which is the range of light with sufficient penetration and energy. In addition, improved pharmacokinetics and pharmacodynamics make chlorin derivatives perfect PSs for PDT [1].



Figure 2. The chemical structure of chlorin e6 (Ce6).

Different approaches have been considered to improve the physicochemical and pharmacological parameters of chlorins. Nishie et al. conjugated chlorin molecules with glucose chains to improve their selectivity against gastrointestinal cancers, while Borbas et al. modified the structure of the original chlorin molecule to increase its water solubility [2,8]. When it is not possible to improve the physicochemical parameters of chlorin molecules using chemical modifications, a solution that can help overcome this problem is the use of combinations of chlorins with nanoparticles [9]. The conjugation between metallic nanoparticles and porphyrinoid-type PSs, such as chlorins, is a field of great interest because nanocarriers can overcome most of the limitations of classic PSs in PDT [10]. Many possibilities have so far been considered, such as the direct functionalization of PS with monoclonal antibodies or specific tumor-targeting molecules (proteins, peptides, and aptamers) [11,12]. Photoactive porphyrinoids can be connected to several types of nanoparticles, including gold, titanium(IV) oxide, magnetic and upconverted nanoparticles, quantum dots, and metal-organic frameworks, to enhance the photocatalytic activity required in PDT or PACT [13,14]. Therefore, contrary to classic drug delivery systems, the release of active PSs by metallic nanoparticles is not always required [10]. It is worth noting that nanoparticle surfaces can be modified with various functional groups, targeting agents, and components, including imaging agents, drugs, targeting ligands, and agents preventing their interference with the immune system. Such combinations are known to reveal many advantages. These are, in no specific order, an increase in the PS biodistribution, improved pharmacokinetics, and cell uptake, as well as targeting abilities around the tumor tissue and hampering the rapid elimination of PS accompanied by possible deactivation with plasma components. In addition, such combinations can prevent the unwelcome accumulation of PS in healthy tissue. Many nanoparticles can increase the amphiphilicity of PSs leading to better distribution through the cardiovascular system and enabling the enhanced permeability and retention effect (EPR) [11].

Among many types of porphyrinoids, various chlorin-type derivatives/metallic nanoparticle hybrids were recently investigated for imaging and therapeutic purposes. This review focuses on Ce6 in conjugation with gold and silver nanoparticles, magnetic, ZnO, TiO_2 nanoparticles, metal-organic frameworks (MOFs), and upconverting nanoparticles (UCNs). Examples of such nanoparticles presented in the scientific literature between 2010 and 2023 were collected with special emphasis on their applications in nanomedicine with a particular focus on PDT, PACT, PTT (photothermal therapy), and tumor tissue imaging. This study can also be considered a continuation of the lately published review, where the conjugates of metallic nanoparticles with BODIPY dyes—structurally different PSs—were presented [15].

2. Metallic Nanoparticles in Conjugation with Chlorin Derivatives

The following review is divided into subchapters regarding the type of nanoparticles used in conjugation with chlorin derivatives. Below each subchapter, the presented data are summarized in bullet points and tables, with information about size, synthetic methods, irradiation wavelengths, light powers/doses (if specified), and in vitro cell viabilities provided.

2.1. Iron Oxide and Other Magnetic Nanoparticles

Magnetic nanoparticles constitute one of the most frequently used metallic nanoparticles as drug delivery carriers. The surface coating for magnetic nanoparticles can be polyvinyl alcohol (PVA), dextran, polyethylene glycol (PEG), polyvinylpyrrolidone (PVP), or chitosan, which protect them from instant clearance within the bloodstream. There are many examples of magnetic nanoparticles with various chlorin conjugates with potential medical applications. An interesting example in this regard was proposed by Di Corato et al., who prepared liposome–cargo particles (Figure 3) bearing iron oxide nanoparticles and a chlorin-based PS—temoporfin. Such a combination can be considered a further development of Foscan, a commercially available liposome formulation. Due to the combi-

nation of iron oxide nanoparticles and temoporfin, such a combination could be applied for magnetothermal treatment (MHT) and PDT [16]. The authors confirmed the stability of nanoparticles within 30 days of storage and later tested it, using an in vitro model, against ovarian cancer cells. The maximal iron uptake was achieved after a 1 h incubation, reaching 15–20 pg per cell. The studies indicated that iron nanoparticles were deposited in the membrane compartment and did not cross this barrier into the cytoplasm. Foscan crossed lipid bilayers and localized inside the cells due to its hydrophobic nature. The authors examined the potential of the combined magneto-phototherapy. They noted that only 10% of the cell population survived when treated with the magnetic field, whereas only 1% persisted when PDT was applied alone. Combining these modalities provided the complete elimination of the initial cell culture population. In parallel, the authors overlooked the impact of nanoparticles on cells when they were not activated. Additionally, the high potential of this liposome cargo was confirmed in in vivo trials using a mouse model. Particles were injected into the tumor, where the majority remained. Non-activated particles did not reveal any impact on the tumor, whereas turning on magnetotherapy and phototherapy alone induced partial cancer regression. Total regression was noted when both therapies were combined. It is believed that magnetotherapy potentiates PDT by increasing the tissue temperature. A higher temperature is the cause of blood vessel extension, thus improving blood flow through the tumor. Increased blood flow provides a higher partial molecular oxygen content in the tumor and its neighborhood. It is essential because molecular oxygen is a substrate for the excited PS in the photodynamic reaction, which leads to the formation of singlet oxygen—a highly reactive agent responsible for cancer cell death [16].

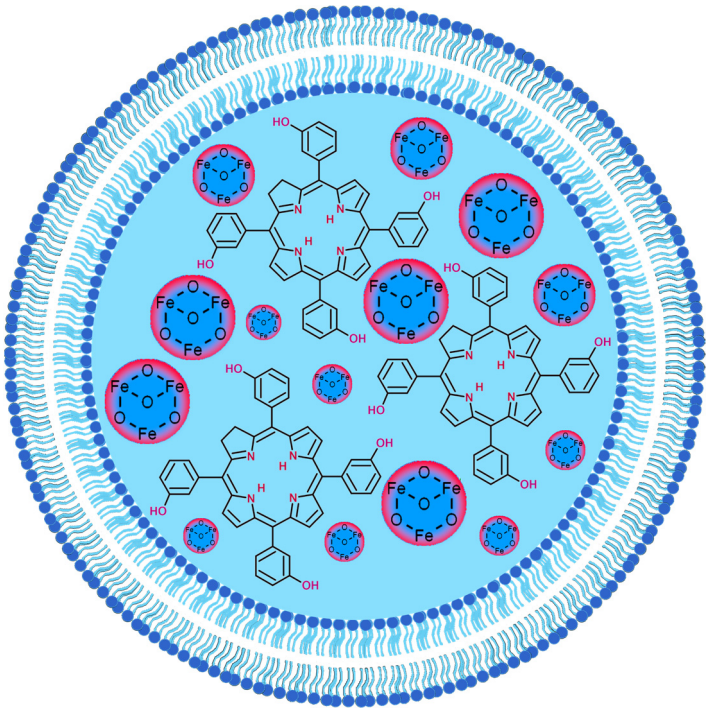


Figure 3. The schematic structure of the liposome–cargo magnetic particles with Foscan [16].

In another study, the theranostic properties of metallic nanoparticles bearing a PS were assessed by Huang et al., who developed nanoparticles consisting of iron oxides (Fe_3O_4) and Ce6 bonded together via an aliphatic linker (Figure 4) [17]. The authors confirmed the formation of singlet oxygen under particle irradiation. The system was applied in in vitro and in vivo studies based on gastric cancer cells and tumors (MGC803). The nanoparticles, at a concentration of 42 μM and excited with light at 632.8 nm with an energy density of 30 mW/cm^2 for 10 min, caused a decrease in cancer cell viability to <20%

of the initial population. Moreover, the nanoparticles enabled cancerous visualization via NIR fluorescence and magnetic resonance imaging (MRI). Particles produced reasonable magnetic responses useful for MRI imaging, which was confirmed in a trial with a nude mouse model [17].

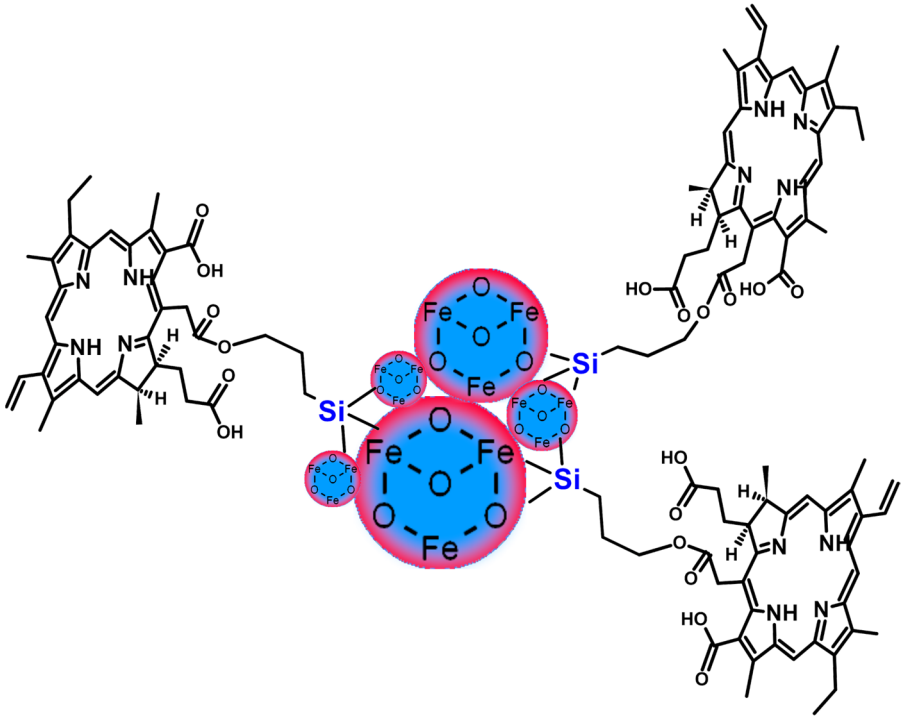


Figure 4. Chemical structure of the Fe_3O_4 nanoparticles that were modified with Ce6 molecules through alkyl chains [17].

Various methods were used for the conjugation of PSs to magnetic nanoparticles. Quite a simple approach was proposed by Amirshaghaghi et al.—they sonicated a mixture of Fe_3O_4 nanoparticles and Ce6 in a toluene/water emulsion [18]. This procedure yielded 92 nm diameter nanoclusters of Fe_3O_4 stabilized in water by the excellent loading of Ce6 molecules assembled on their surface (also reaching over 50% of the mass of the nanoclusters). The material was tested in vivo based on athymic nude mice bearing xenograft breast cancer tumors (4T1 cell line) and tended to accumulate in tumors upon intravenous injection. Due to the paramagnetic properties of the Fe_3O_4, the nanoclusters could be used as a contrast agent in MRI, and although the fluorescence from Ce6 was quenched in solution, the nanoclusters in vivo exhibited increased fluorescence and enabled fluorescence imaging. Another property of this material was related to its ability to generate singlet oxygen, which allowed for the performance of the PDT experiment in vitro in the dark conditions on 4T1 cells and healthy human umbilical vein endothelial cells (HUVECs). The material was found to be non-toxic without irradiation. The viability of 4T1 cells, which were irradiated with a 665 nm laser, was lower than 10% compared to that of the non-irradiated cells. The in vivo PDT experiment showed a significant decrease in the tumor volume in mice in which nanoclusters were administered compared to Ce6-treated mice [18].

Another method was proposed by Yang et al., where a complex nanocluster material, by combining poly(isobutylene-alt-maleic anhydride), PEGs, dopamine, cystamine, Ce6, and Fe_3O_4 nanoparticles, was prepared [19]. The nanosystems were studied for their in vitro PDT utility based on MDA-MB-231 cells (metastatic mammary gland adenocarcinoma) and were found more effective than Ce6 alone. The same effect was also observed in the in vivo experiment using mice bearing MDA-MB-231 cell line tumors. The authors suggested that the obtained material can be useful for in vivo MRI and fluorescent imaging [19].

The coordination of Ce6 to iron atoms on the surfaces of magnetic nanoparticles coated with glucose was proposed by Yu et al. to improve the distribution of Ce6 in lung cancer [20]. The in vitro and in vivo studies performed with the Lewis cell line (LLC) and an LLC-tumor-bearing mouse model revealed that the obtained nanosystems significantly damaged the DNA code of the lung cancer cells and activated the mechanism of augmented immunogenicity leading to tumor cell death. McCarthy et al. conjugated a novel unsymmetrically substituted chlorin, also with dextran-coated iron oxide nanoparticles [21]. The intent was to propose a new method of atherosclerosis treatment. The material was initially tested for its non-toxicity in dark conditions using RAW 264.7 murine macrophages, and when confirmed, it was applied in vivo to apolipoprotein E-deficient mice, which were fed a high-cholesterol diet. The material was primarily found to accumulate in the inflammatory macrophages and exhibited significant photocytotoxicity (LD_{50} = 14 nM). It was concluded that the material shows promising features for stabilizing arteriosclerotic lesions [21].

The Fe_3O_4 magnetic nanoparticles were also successfully functionalized with aptamers, graphene oxide, Ce6, and paclitaxel for the selective killing of MCF-7 tumor cells, by Işıklan et al. [22]. The researchers proved that the photothermal impact of the fabricated nanocomposite could be used to perform the Ce6 release when irradiated to a near-infrared laser at a low-power density. A synergistic therapeutic effect was observed when 660 and 808 nm lasers were used, significantly enhancingMCF-7 cell death (83.67%).

Bovine serum albumin-coated iron peroxide nanoparticles conjugated with Ce6 was invented by Hu et al. [23]. BSA coating was responsible for improving biocompatibility and prolonging the internal circulation time, while iron cations can induce the chemodynamic therapy effect by reacting with overexpressed hydrogen peroxide in the tumor to produce cytotoxic hydroxyl radicals. What is more, they can increase the glutathione uptake in the tumor cells. The size of the obtained nanoparticles via electrostatic adsorption and hydrophobic interactions was about 197.5 nm. The in vitro and in vivo studies on murine breast cancer cells and tumor-bearing mice revealed an excellent cytotoxic effect (cell viability at 3% in in vitro studies) after irradiation with light at 660 nm, a standard wavelength for PDT with the use of Ce6 [23].

Interesting nanoparticles, named pH-sensitive magnetic nanogrenades (PMNs), were presented by Ling et al. [24]. Designed nanostructures consisted of chain poly(ethylene glycol)-poly(β-benzyl-L-aspartate) ligands bearing a PS—Ce6 and an imidazole ring sensitive to pH changes. The type A ligands with catechol groups were bound to iron oxide nanoparticles with a dimension of ca. 3 nm, unlike the type B ligands with phenol groups. The PMN particles with a hydrodynamic diameter of 70 nm were well-dispersed in water and consisted of a hydrophobic core with Ce6 ligands and a spherical-shaped PEG shell. The MRI experiments indicated that at pH 7.4, the MR contrast is quenched, whereas it is significantly enhanced at pH 5.5. Thus, the authors concluded that the obtained material could be considered a highly selective cancer imaging tool. Simultaneously, the authors assessed the cellular uptake of PMNs by human colorectal carcinoma (HCT116). Higher uptake of PMNs was noted at pH 6.8 than at pH 7.4. In in vivo experiments, the authors observed the potential of the material for early-stage tumor visualization and noted the cancerous changes of ca. 3 mm in diameter. Moreover, prolonged blood circulation with a $t_{1/2}$ value of 2.9 h was noted. The authors also indicated the possibility of applying PMNs for cancer treatment based on the mouse model bearing a homogeneous HCT116 xenograft and for the treatment of highly heterogeneous, drug-resistant CT26 tumors [24].

The combination of magnetic and carbon nanoparticles functionalized with Ce6 and platinum atoms was fabricated by Xu et al. for MRI purposes, as well as photodynamic and photothermal effects [25]. The obtained yolk-shell magnetic Fe_3O_4@Carbon@Platinum-Ce6 nanoparticles increased the T2 MRI ability and revealed a high photothermal conversion efficiency and PDT therapeutic effects in acidic and H_2O_2-rich microenvironments in the CT26 tumor-bearing mice, after irradiation with a laser at 660 nm and 808 nm. Moreover, in the obtained nanoparticles, the presence of Pt atoms enhanced the catalytic ability of the

photocatalyst toward the generation of reactive oxygen species by catalyzing the hydrogen peroxide cleavage to O_2 moieties [25].

Photodynamic and magnetothermal therapies were not the only ones where the conjugates of magnetic nanoparticles and chlorins were utilized in biomedical applications. Magro et al. proposed a core-shell hybrid nanomaterial based on maghemite nanoparticles (γ-Fe_2O_3) against *Aedes aegypti* instead of insecticides [26]. The mosquito *Aedes aegypti* is responsible for spreading dengue and yellow fever. Maghemite nanoparticles are materials with an active surface binding specific molecules, including carboxyl group-bearing organic molecules, i.e., Ce6. The authors estimated that for 6 days, the release of the PS was equal to 25%. Nanoparticles were administered to the mosquito larvae in the feed formulates and accumulated in the gut. Exposing nanoparticles at concentrations 50 and 100 mg/L to the light for 3 and 1.4 h, respectively, caused 100% larvae mortality. Simultaneously, studies on eco-toxicity for aquatic microorganisms were performed. The authors observed no toxic effect against *Daphinia magna* under the same conditions used against mosquitos. Water plants *Pseudokirchneriella subcapitata* and *Lemna minor* were also treated with the developed nanoparticles, and again, no impact on their growth was noted [26]. The data described in Section 2.1 are summarized in Table 1.

In summary:

- Most magnetic nanoparticles used were Fe_3O_4 conjugated with Ce6 via silica or dextran coatings or incorporated into a polymer structure.
- The conjugates of chlorins and magnetic nanoparticles allowed for efficient combined magnetothermal–photodynamic treatment after laser irradiation at 660 and 808 nm.
- The promising theranostic features of the Fe_3O_4-chlorin conjugates can be used for photodynamic therapy and MRI or fluorescent imaging.
- Different types of connections in the obtained conjugates were used, including core-shell structures, liposomes, polymeric nanoclusters, and covalent bonding.

Table 1. A summary of the data presented in Section 2.1.

Type of NPs	Size of NPs	Preparation Method	Wavelength [nm]	Light Dose/Light Power	Cell Type	Cell Viability	Ref.
Fe_3O_4 (loaded in liposomes)	150 nm	alkaline co-precipitation of $FeCl_2$ and $FeCl_3$	650	5 or 10 J/cm^2	human adenocarcinoma SKOV-3 cells	0.2% at 5 J/cm^2 and 0% at 10 J/cm^2	[16]
Fe_3O_4	20 nm	coprecipitation of Fe^{2+} and Fe^{3+} in the presence of $NH_3 \times H_2O$	632.8	30 mW/cm^2	MGC803 cells	40% at 25.2 µM; 80% at 42 µM	[17]
Fe_3O_4	92 nm	thermal decomposition method	665	5 J/cm^2	4T1 cells	<10%	[18]
Fe_3O_4	90 nm	thermal decomposition method	660	N/A	MDA-MB-231 cells	approx. 20%	[19]
Fe_3O_4	220 ± 30 nm	reaction of tris(acetylacetonate) iron with tri(ethylene) glycol at 300 °C for 2 h	690	0.5 W/cm^2	Lewis cells	approx. 0.5%	[20]
Dextran-coated Fe_3O_4	49.9 nm	crosslinking of the dextran coating around the iron oxide core	650	150 mW/cm^2 (6 J/cm^2)	murine macrophage RAW 264.7 cells	0% (LD_{50} of 14 nM)	[21]
Aptamer and GO-functionalized Fe_3O_4	10 nm (bare Fe_3O_4)	thermal decomposition method	660 and 808	100 mW/cm^2 for 660 nm	MCF-7 tumor cells	16.33%	[22]

Table 1. *Cont.*

Type of NPs	Size of NPs	Preparation Method	Wavelength [nm]	Light Dose/Light Power	Cell Type	Cell Viability	Ref.
FeOOH	197.5 ± 8.2 nm	hydrothermal method	660	5.8 mW/cm^2	murine breast cancer cells 4T1	3%	[22]
Magnetic nanogrenades	60 nm	thermal decomposition of an iron−oleate complex in the presence of oleyl alcohol	670	5 mW/cm^2	HCT116 cancer cells	approx. 10%	[24]
Fe_3O_4	15 nm (bare Fe_3O_4)	thermal decomposition of an iron−oleate complex in the presence of ethanol and 1-octadecene	660 and 808	346 mW/cm^2 for 660 nm and 1 W/cm^2	CT26 colon cancer cells	3.01%	[25]
γ-Fe_2O_3	11 ± 2 nm	chemical reduction of $FeCl_3$ by $NaBH_4$ in alkaline media	constant white light (no specific wavelength)	N/A	mosquito larvae	average mortality after 5 h— 74.3 ± 36.8%	[26]

2.2. Gold Nanoparticles

Due to the plasmon resonance and possible surface functionalization, gold nanoparticles constitute good nanocarriers for PSs, such as chlorins, and enhance the photodynamic effect of the obtained nanosystem. Several studies, as discussed below, indicate their interesting potential for PDT. For example, Zhang et al. presented the potentiation of singlet oxygen formation by Ce6 via plasmon resonance energy transfer (PRET) from gold nanostructures [27]. The PS was deposited on gold nanorods via electrostatic interactions. Under 660 nm light irradiation, the 10-fold increase in singlet oxygen production by PRET-Ce6 nanoparticles was noted compared to that with free Ce6. In addition, high singlet oxygen production was detected within MDA-MB-231 cancer cells. Moreover, over a 2-fold higher cell viability reduction for PRET-Ce6, compared to that with Ce6, was observed [27].

The simplest conjugation of gold nanoparticles and Ce6 based on the physical adsorption of Ce6 on the surface of the gold nanoparticles (AuNPs) was proposed by Tian et al. [28]. The obtained material demonstrated low photoactivity in the isolated form, whereas significant fluorescence and PDT activity was observed for the aggregated form. The authors irradiated the in situ aggregated nanoparticles inside HeLa cancer cells with red and near-infrared light. They obtained excellent PDT and PTT performance, leading to the effective eradication of cancer cells with a killing efficacy of up to 76%, in comparison to 25% with aggregated bare AuNPs and 32% with the use of isolated Ce6 [28].

The enhancement of cancer cell treatment by a combination of photothermal and photodynamic therapy was reported by Gao et al. [29]. These authors developed Au nano cup-based nanoparticles bearing Ce6 as a PS. Chlorin was bound with a nano cup via a polyethylene glycol (PEG) chain, anchored to gold by sulfur and chlorin by an amide bond. It was observed that nanoparticles activated with light at 660 nm (for PDT) and 808 nm (for PTT) reduced HeLa cell viability to 10.3%, compared with 67.5% for PDT and 48.2% for PTT when used separately. Simultaneously, the experiment with no light activation was performed. In the dark conditions, no impact on the viability of the cells was noticed. The photothermal effect in the solution, observed after the irradiation of nano cups with light at 808 nm and dose 150 J/cm^2, revealed an increase in the sample temperature up to 67 °C. Moreover, in vivo trials were performed using a nude mouse model with a subcutaneous HeLa tumor. After 24 h from intravenous nanoparticle injection, the authors observed excellent visualization of the tumor via photoacoustic and computed tomographic techniques. Moreover, they performed PDT and PTT and noted that the combined methods

provided total tumor remission, whereas PDT and PTT separately led only to a partial response [29].

Wu et al. performed a synergistic photothermal and photodynamic cancer therapy using gold nanoflowers conjugated by glutathione moieties with Ce6 and finally coated with polydopamine obtained via the self-polymerization of dopamine [30]. In the in vitro and in vivo studies performed based on female BALB/c mice with HeLa cells, using combined 660 and 808 nm laser irradiation, excellent phototoxicity and synergistic effects of the obtained multifunctional material in killing cancer cells were observed.

The activity enhancement was also noted for PDT/PTT bacteria inactivation. Gil-Tomás et al. obtained gold nanoparticles conjugated with a tin complex of chlorin e6 via a glutathione linker (Figure 5) [31]. The authors excited nanoparticles with white light and achieved ca. 2 logs of growth reduction for *Staphylococcus aureus* at the concentration of 28.8 nM, whereas the PS only provided the same result at the concentration of 50 μM [31].

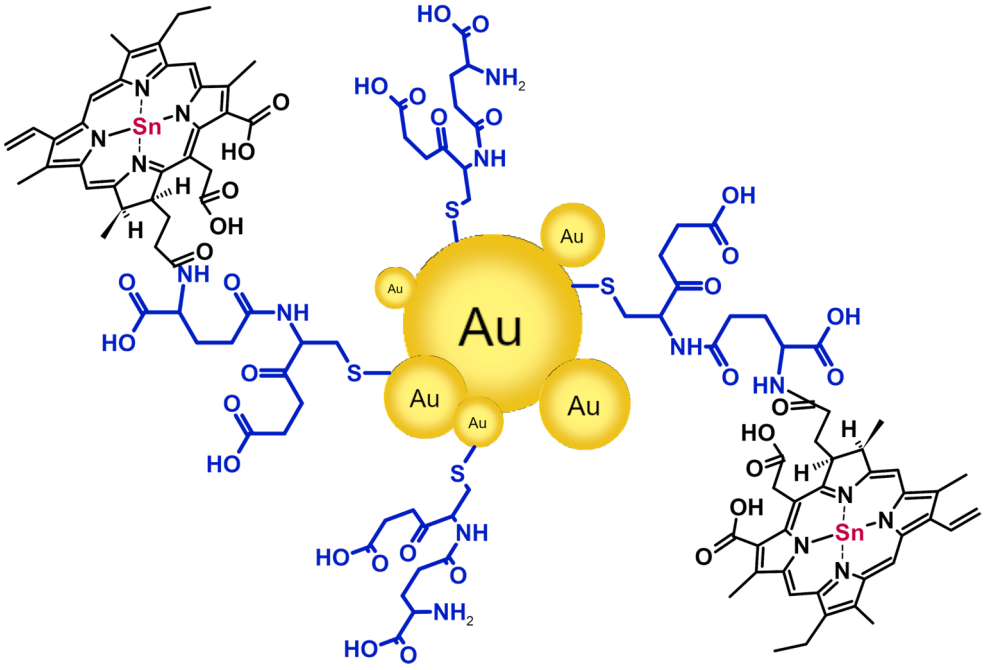


Figure 5. Chemical structure of the conjugate consisting of tin chlorins (black), glutathione linkers (blue), and gold nanoparticles (yellow) [31].

Vieira et al. also noted the enhanced activity of nanogold particles linked with Ce6 in comparison to that of separately used ingredients [32]. These authors covalently linked thiourea to the carboxy group of Ce6. The obtained chlorin derivative was connected to the 18 nm gold nanoparticles through the sulfur atoms of the thiourea moieties. The obtained nanoparticles were tested against the human breast carcinoma cell line MDA-MB468 and revealed high biocompatibility without irradiation, as almost 100% of cancer cells survived incubation with nanoparticles. However, irradiating nanoparticles with light at 660 nm reduced viable cells to 0%, whereas when Ce6 alone was used, the loss of cancer cell viability was less significant [32]. Worth mentioning is the fact that when unmodified Ce6 was used to graft gold nanoparticles, almost no difference was found, which indicates that in this case, the modification with urea does not play a role in in vitro activity. The authors emphasized that the differences might appear more evident for the materials tested in vivo.

Gold nanoparticles were also studied in theranostics, where the photodynamic activity of conjugates was used in both PDD and PDT. Such multimodal theranostic nanoparticles were designed by Sun et al. [33]. They utilized a gold nanorod dimer with attached Ce6 for photothermal and photodynamic therapy, as well as for upconversion of luminescence, magnetic resonance, photoacoustic, and computed tomography imaging modalities.

Firstly, two gold nanorods were linked by two complementary oligonucleotides and formed nanorod dimers. Further Yb, Er-doped $NaGdF_4$ upconversion nanoparticles were connected with Ce6 by an oligonucleotide. Next, the nucleotide linker was introduced to the nanorod dimers to bind the previously obtained upconversion nanoparticles with Ce6. The activity of the developed nanosystem was studied in vitro using HeLa cells. In the TEM analysis, the attachment of HeLa cells around the dimer nanosystem was observed. Irradiation of the system with light at 980 nm provided the photodynamic response, which, when used immediately after 808 nm irradiation, also gave a photothermal effect. The combined PDT/PTT effect caused 0% HeLa cell viability in the in vitro studies, whereas only a partial response was achieved when PDT and PTT were utilized separately. For the in vivo experiments, a nude mouse model bearing a HeLa tumor was applied. Nanoparticles were administered via injection into the tail vein, and first, the designed system was studied in terms of imaging. Bright images of the tumor were recorded after 24 h of accumulation. The multimodal diagnostic features, as well as the treatment efficacy, were confirmed. Irradiation with 980 nm was performed for PDT. Next, the PTT effect was studied when the irradiation source was switched from 980 nm to 808 nm. This time, a significant decrease in tumor volume was also noted. Simultaneously, no body weight loss was observed, and nanoparticles within 15 days were wholly eliminated [33].

Another example of a theranostic approach with gold nanoparticle/chlorin conjugates was presented by Castilho et al. [34], who prepared 21 nm gold nanoparticles functionalized with Ce6 and epidermal growth factor (EGF). The in vitro studies performed with the MDS-MB-468 and MCF-10 cell lines revealed that the obtained bifunctional theranostic nanoprobes were highly cytotoxic to cancer cells (86%) with no toxic effect on normal cells. It was also found that with the most effective concentration of 0.2 μg/mL, nanoprobes caused both necrosis and apoptosis to tumor cells with a ratio of 3:2.

Some benefits of combining gold nanoparticles with Ce6 were underlined by Yeo et al. [35]. These authors applied human serum corona protein to cover gold nanorods previously covalently bound with Ce6 via the sulfur bridge. In the in vitro experiments with CAL 27 oral squamous cell carcinoma, 95.2% of dead cells were observed in the treated culture. It is worth mentioning that the authors used nanoparticles at an extremely low concentration of 50 pM corresponding to 7.67 μg/mL of Au and 4.83 nM of Ce6. Moreover, a 57-fold increase in the cellular uptake of Ce6-loaded nanoparticles compared to that with bare Ce6 was observed [35].

The studies of the theranostic systems involving gold nanoparticles and chlorins were continued by Huang et al. [36], who developed a photo-theranostic agent for PDT and PDD. The gold nanoparticles linked with an aliphatic linker with Ce6 generated singlet oxygen under illumination, significantly reducing living melanoma MDA-MB-435 cells in the in vitro experiment. The authors found that the gold-based nanoclusters entered the cells based on the endocytosis pathway and spread within the cytoplasm, whereas some particles entered the lysosomes. The preferential accumulation of the system in cancerous tissue and high light emission allowed them to consider the nanoparticles for visualization of the tumor [36].

Yu et al. utilized pH Low Insertion Peptide (pHLIP) to insert attached gold nanoparticles bearing Ce6 into the cells upon decreased pH [37,38]. Firstly, PEG was introduced to the gold nanoparticles, and then, particles were modified with amine groups. Finally, Ce6 and pHILP were adsorbed onto hollow gold nanospheres via electrostatic forces. The physicochemical, in vitro, and in vivo experiments allowed them to conclude that the nanoagent under excitation with light efficiently forms ROS and generates a photothermal effect. The translocation of the nanoparticles into a liposomal sphere through the interaction of pHILP with membrane lipids was confirmed using the liposomal model. Translocation into cells occurred only when the pH value decreased from neutral 7.4 to the typical acidic pH for most cancer tissues, around 6.2. Moreover, it was found that upon irradiation, the generated heat caused the disintegration of gold nanospheres and Ce6. In the in vitro experiments on HeLa cells, the authors observed a significant decrease in cell viability upon

irradiation. In vivo tests indicated significant inhibition of tumor growth measured after three weeks. The possibility of cancer imaging based on photothermal and fluorescence phenomena was confirmed [37,38].

Aside from Ce6, some other chlorin derivatives were utilized in conjugations with diverse gold nanoforms. Haimov et al. prepared gold nanoparticles with a diameter 12 nm linked to *meso*-tetrakis(3-hydroxyphenyl)chlorin (mTHPC) using 3-mercaptopropionic acid [39]. It was found that after conjugation to gold, the singlet oxygen generation quantum yield was slightly lower than that noted for the chlorin only. Conversely, the in vitro experiments using SH-SY5Y human neuroblastoma cells indicated that conjugation of the chlorin to gold nanoparticles increased their photocytotoxicity. Additionally, the combination with gold nanoparticles significantly decreased the dark toxicity of mTHPC at higher concentrations [39].

A combined photothermal and photodynamic effect was obtained with good results for CeO_2-coated gold nanorods encapsulated within a temperature-sensitive polymer structure and conjugated with Ce6 [40]. The near-infrared irradiation at 808 nm caused an increase in the temperature up to 60 °C resulting in significant tumor tissue ablation. What is more, at 50 °C, the cumulative release rate of Ce6 was 95.31%. The CeO_2-coating effectively alleviates the anaerobic tumor microenvironment, which was proven in in vitro and in vivo tests on HepG2 cells and tumor-bearing mice [40].

Thiolated chlorin derivatives were also adsorbed on the surface of the bimetallic gold–platinum nanoparticles by Magalhães et al. [41]. The obtained conjugates displayed lower dark cytotoxicity in in vitro studies based on the murine melanoma cell line B16F10-Nex2. In addition, higher generation of singlet oxygen and cell internalization compared to those with unmodified chlorin conjugated to bare AuNPs was observed.

An interesting nanomaterial based on gold/Ce6 nanoclusters targeted with folic acid was prepared Zhang et al. [42]. In the first step, the authors fabricated gold nanoclusters with a diameter of ca. 2 nm. In the next step, the polyethylene glycol (PEG) chains linked to the folic acid and bearing anchor NHS groups were conjugated with gold nanoparticles. Finally, the photosensitizer Ce6 was introduced into hydrophobic pockets formed by PEG. The authors assessed cellular uptake into gastric cancer cells with an overexpressed folic receptor MGC-803 and human gastric epithelial folic receptor-negative cells—GES 1 cells. Synthesized gold nanoparticles accumulated 4.8-fold more efficiently in the MGC-803 cells compared to that with Ce6 only, whereas nanoparticles in the normal FR-free GES 1 cells reached a negligible level in contrast to that with free Ce6. Therefore, the authors concluded that the developed therapeutics are highly selective. It was confirmed that the introduction of Ce6 into the PEG-pockets within the nanoagent did not decrease the ability of singlet oxygen formation in comparison to that with the free Ce6. In dark conditions, only low cytotoxicities of Ce6@GNC-PEG-FA, similar to those of the bare nanogold and Ce6 only, were reported. It is worth noting that upon irradiation with 633 nm, nanoparticles produced 2–3 times more dead cancer cells than the free Ce6. Pharmacokinetic parameters were also evaluated using an in vivo BALB/c mouse model. Synthesized nanoparticles followed two-compartment pharmacokinetics. Distribution half-life time and an elimination half-life time values were determined and were equal to 0.17 and 20.49 h, respectively. In the in vivo test, the significant inhibition of tumor growth after irradiation of the administrated nanoparticles at 633 nm was observed. The authors also checked the influence of presented gold nanoclusters on mice. They performed hematoxylin and eosin staining. This test indicated no changes within crucial organs, i.e., the liver, heart, kidney, and brain. Moreover, the biochemistry analyses of liver and kidney function were evaluated. All tested probes revealed no toxicity; thus, the studied nanoparticles seemed to constitute promising candidates for selective efficient cancer treatment [42].

The deep location of some tumor tissues and the low ability of light to penetrate biological tissues are the main obstacles in modern PDT. For this reason, new methods of ROS production have to be developed. One of them is sonodynamic therapy (SDT), where an alternative excitation source instead of light—ultrasound—has been implemented. As an

external excitation source, ultrasound demonstrates some advantages of less invasiveness, deeper penetration, a wider range, and lower cost compared to PDT [43,44]. Following this line of thinking, the pH-sensitive silica-coated gold nanoparticles encapsulated within a phospholipid carrier and conjugated with Ce6 were fabricated and used in SDT as a first example of a sonosensitizer based on gold NPs and chlorin. What is more, the obtained material was further conjugated with doxorubicin hydrochloride. The in vitro and in vivo studies against C26 and 3T3 cells and mice with orthotopic colorectal tumors revealed good cytotoxic effects when classic chemotherapy was combined with SDT [43].

Despite PDT-targeted anticancer approaches, numerous studies related to the photodynamic inactivation of bacteria have been performed. The potentiation effect of a PS doped onto nanometallic particles against bacteria was confirmed by Wijesiri et al. [45]. The authors attached an amphiphilic block copolymer—poly(NIPAAm-*b*-styrene)—to the gold nanoparticles. The hydrophobic part of the polymer was linked to the gold nanoparticles via a sulfur atom, whereas the hydrophilic part was oriented outside the particle. Consequently, the hydrophobic pockets inside the nanoparticles were formed, onto which hydrophobic Ce6 was loaded. Developed nanogold particles with Ce6 were stable over weeks. The block copolymer allowed for the dispersion of nanoparticles in the water environment. The biocompatibility of nanoparticles was evaluated. Therefore, nanoparticles were incubated with MCF-7 cells, and their viability was assessed as above 80%. Next, the authors evaluated the potential for the photoinactivation of methicillin-resistant *Staphylococcus aureus*. Irradiation with white light at a dose of 73 J/cm^2 of the bacterial cultures incubated previously with nanoparticles demonstrated ca. 6 log inactivation rate, higher than that with Ce6 only or gold nanoparticles bearing an amphiphilic block copolymer [45]. The data described in Section 2.2 are summarized in Table 2.

Table 2. Summary of the data presented in Section 2.2.

Type of NPs	Size of NPs	Preparation Method	Wavelength [nm]	Light Dose/Light Power	Cell Type	Cell Viability	Ref.
Gold	52.2 ± 6.3 nm	chemical reduction of $HAuCl_4$ by $NaBH_4$	660	53 mW/cm^2	MDA-MB-231 cancer cells	approx. 25%	[27]
Gold	13 nm	aqueous reduction of $HAuCl_4$ with trisodium citrate using the Turkevich–Frens method	660	194 mW/cm^2	HeLa cells	24%	[28]
Gold nanocups	124 ± 4 nm	chemical reduction of $HAuCl_4$ by ascorbic acid in PbS nanooctahedron suspension	660 and 808	10 mW/cm^2 for 660 nm and 0.5 W/cm^2 for 808 nm	HeLa cells	10.3 ± 1.4%	[29]
Gold nanoflowers	80 nm	chemical reduction of $HAuCl_4$ by ascorbic acid and further treatment with $NH_2OH{\cdot}HCl$	660 and 808	100 mW/cm^2 for 660 nm and 2 W/cm^2 for 808 nm	HeLa cells	13%	[30]
Glutathione coated gold	5.6 ± 1 nm	chemical reduction of $HAuCl_4$ by $NaBH_4$ in acidified methanol	20 W halogen bulb cold light (620–700 nm)	N/A	*Staphylococcus aureus Streptococcus pyogenes*	2 log reduction at conc. of 2.88×10^{-8} M	[31]
Gold	18 ± 4 nm	aqueous reduction of $HAuCl_4$ with trisodium citrate using the Turkevich–Frens method	660	25 mW/cm^2 (25 J/cm^2)	human breast carcinoma cells MDA-MB-468	0% in conc. range 0.16–1.67 μM	[32]

Table 2. *Cont.*

Type of NPs	Size of NPs	Preparation Method	Wavelength [nm]	Light Dose/Light Power	Cell Type	Cell Viability	Ref.
Gold nanorods dimers/upconverted nanoparticles	~40 nm	gold seed-mediated growth method	808 and 980	0.2 W/cm^2 for 808 nm and 2 mW/cm^2 for 980	HeLa cells	0%	[33]
EGF-functionalized gold NPs	21 nm	conventional sodium citrate reduction of gold chloride	660	25 mW/cm^2 (25 J/cm^2)	human breast carcinoma cells MDA-MB-468	14%	[34]
Human serum corona protein-coated gold nanorods	46.5 ± 1.2 nm by 19.0 ± 0.7 nm	chemical reduction of $HAuCl_4$ by $NaBH_4$	665	250 mW/cm^2	squamous cell carcinoma (OSCC) cells	4.8%	[35]
Gold	67.93 ± 8.5 nm	chemical reduction of HAuCl4 by ascorbic acid in bovine serum	671	2 W/cm^2	human breast carcinoma cells MDA-MB-435	approx. 5%	[36]
PEGylated gold nanoparticles	119.2 nm	sacrificial galvanic replacement of cobalt nanoparticles based on chloroauric acid	670 and 808	2 W/cm^2 for 808 nm	HeLa cells	approx. 25%	[37,38]
Gold	12 ± 1 nm	aqueous reduction of $HAuCl_4$ with citrate using the Turkevich–Frens method	650	1 J/cm^2	SH-SY5Y human neuroblastoma cells	0% at Ce6 conc. 0.64 µM	[39]
CeO_2-coated gold nanorods	55 nm	chemical reduction of HAuCl4 by $NaBH_4$ in presence of CTAB, $AgNO_3$, and $NH_2OH \times HCl$	660 and 808	N/A	HepG2 cells	<20%	[41]
Bimetallic gold–platinum NPs	19 ± 8 nm	aqueous reduction of $HAuCl_4$ with trisodium citrate using the Turkevich–Enustun method	660	102 J/cm^2	murine melanoma cell line B16F10-Nex2	14%	[41]
Folic acid functionalized gold nanoclusters	6.1 ± 1.2 nm	modified TBAB-reduction method (aqueous reduction of $HAuCl_4$ with tetrabutylammonium borohydride)	633	100 mW/cm^2	human gastric carcinoma cell line MGC-803 cells	10%	[42]
Silica-coated gold nanoparticles	61.21 nm	chemical reduction of $HAuCl_4$ by sodium citrate in presence of CTAB	Not applicable—sonodynamic therapy	Not applicable—sonodynamic therapy	orthotopic colorectal tumor C26 and 3T3 cells	<50%	[44]
Poly(NIPAAm-*b*-styrene/gold nanoparticles copolymer	~40 nm	aqueous reduction of $HAuCl_4$ with trisodium citrate	white light	408 mW/cm^2 (73 J/cm^2)	*Staphylococcus aureus*	7 log reduction	[45]

In summary:

- Gold nanoparticle@chlorin conjugates were studied regarding the PRET phenomenon and photothermal and photodynamic effects to assess their prospective biomedical applications.
- For Ce6, the laser irradiation wavelengths used for PDT purposes were in the range of 633–671 nm due to the different structures of obtained conjugates.
- Most conjugates between Ce6 and nanogold were based on covalent bonding via various molecules, such as glutathione, thiourea, oligonucleotide, and 3-mercaptopropionic acid.

- Gold nanoparticles were mainly synthesized via the chemical reduction of $HAuCl_4$ by sodium citrate (the Turkevich method) or $NaBH_4$.
- Depending on the synthetic procedure, various types of gold nanoparticles, including nanorods, nanocups, and nanoflowers, were obtained.
- Polymer coating of the gold nanoparticles allowed for the formation of inclusion complexes with Ce6.

2.3. Upconverted Nanoparticles

Upconverted nanoparticles (UNs), consisting of host lattices of ceramic materials embedded with transition metals, actinide, or lanthanide ions, such as Yb^{3+}, Er^{3+}, and Tm^{3+}, display a unique feature that is based on a process of the emission of light at a shorter wavelength in comparison to the excitation wavelength after the sequential absorption of two or more photons [46]. The use of upconversion nanoparticles brings one significant advantage—created material can be irradiated with near-infrared (NIR) wavelengths. The energy absorbed is converted and emitted as fluorescence in the visible or UV region upon NIR irradiation. The desired emission wavelength of the photosensitizer can be triggered by appropriately selected doped upconversion nanoparticles. Matching the emission and excitation wavelengths of the two components so that they overlap is critical to unleashing the cascade of energy transfers (Figure 6).

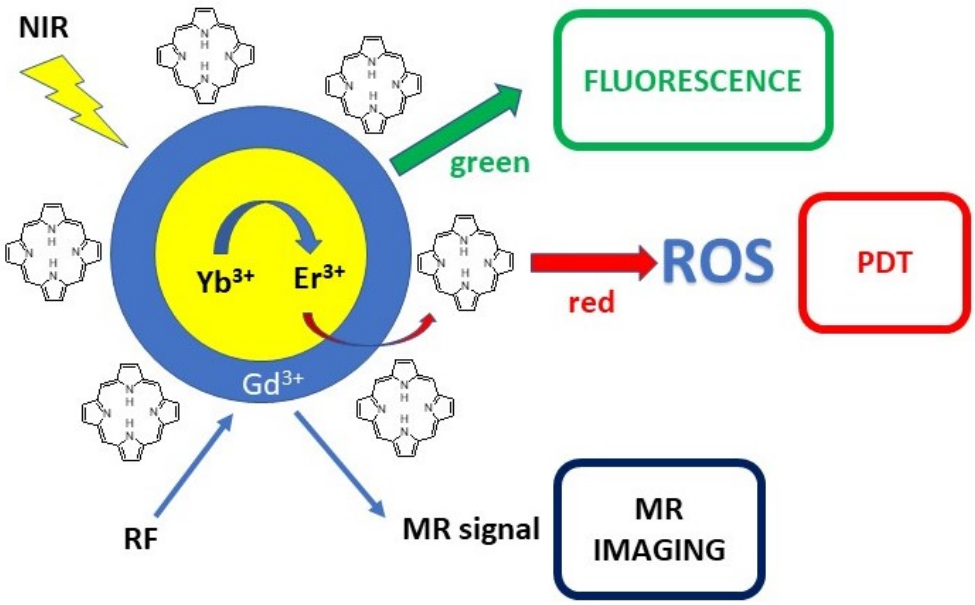


Figure 6. Schematic presentation of energy transfer in UNs–Ce6 conjugates.

Such an approach has received much attention recently. Wang et al., prepared β-$NaYF_4$:Yb, Er(Tm) nanoparticles coated with a PEGylated polymer, functionalized with folic acid for targeting [47]. The material was mainly studied as a vehicle for the enhanced delivery of doxorubicin, but it was also shown to be a suitable carrier for Ce6 and *meso*-5,10,15,20-tetrakis(4-carboxyphenyl)porphyrin (TCPP).

Hexagonal $NaYF_4$:Yb,Er/$NaGdF_4$ core-shell nanoparticles bearing Ce6 were proposed by Park et al. for cancer diagnosis and treatment (Figure 7) [48]. Ce6 molecules were incorporated into the hydrophobic layer surrounding core-shell nanoparticles, which allowed to enhance their water solubility. Moreover, the carboxy groups present in the Ce6 molecules were applied in their conjugation with amino-modified particles with amide bond formation. The mechanism of action of the discussed nanomaterial was based on an upconverting phenomenon. Ytterbium was responsible for light absorption at the wavelength of 980 nm and energy transfer to the Erbium, which produced fluorescence. In addition, the PS Ce6 molecules were excited with the red light emitted by Erbium, which

produced singlet oxygen responsible for cancer cell death. A nanoparticle shell bearing gadolinium ions was responsible for the magnetic resonance signal. The advantage of optical imaging was its sensitivity and the MRI spatial resolution. The authors performed in vitro and in vivo experiments, and for both biological models, noted the high imaging potentialwith significant green emission within the tumor up to 6 h after injection. The authors also noted high biocompatibility with no negative response up to 0.25 mg/mL of rare earth metals. The assessed half-time of designed nanoparticles equaled 21.6 min, and they accumulated in the liver and spleen at a low level. The nano particles applied in vitro against cancer U87MG cells and in vivo, irradiated with light at 980 nm,revealed significant cell death and tumor growth inhibition [48].

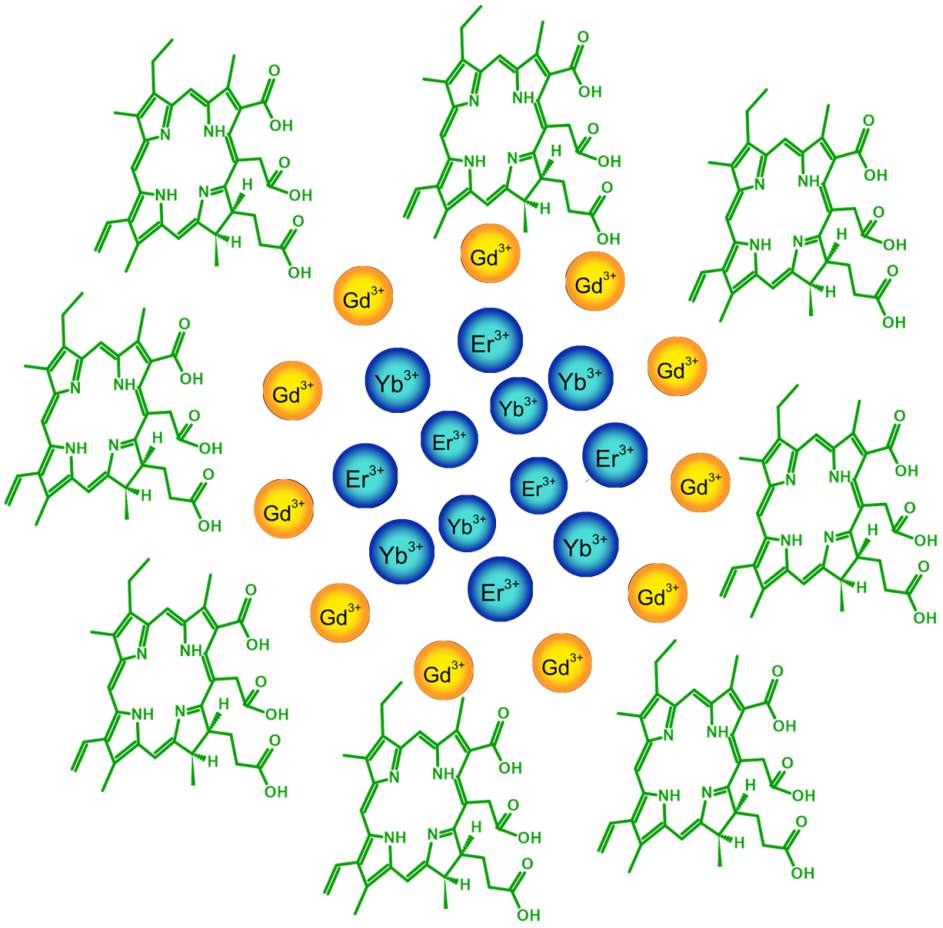


Figure 7. Chemical structure of upconverted nanoparticle/Ce6 conjugates, which were obtained by Park et al. [48].

An interesting photocatalytic material was invented by Zhang et al., who combined the Fe_3O_4/MnO_2-doped $NaYF_4$:Yb/Er/Nd upconversion nanoparticles with black phosphorus nanosheets (BPNs) and linked Ce6 via polyacrylic acid [49]. The material revealed several advantages in in vivo studies with HeLa-bearing mice, of which the most significant arethe following: (*i*) it was activated only with single light at 808 nm leading to the activation of both PTT and PDT mechanisms (catalyzed both by BPNs and Ce6); (*ii*) MnO_2 decomposition overexpressed hydrogen peroxide in the tumor microenvironment leading to the generation of oxygen species enhancing PDT effects; and finally (*iii*) the doped Fe_3O_4 and MnO_2 nanoparticles were able to facilitate T1 and T2 MRI imaging, leading to a multimodal imaging system accompanied by the Ce6 fluorescence imaging [49]. The data described in Section 2.3 are summarized in Table 3.

Table 3. Summary of the data presented in Section 2.3.

Type of NPs	Size of NPs	Preparation Method	Wavelength [nm]	Light Dose/Light Power	Cell Type	Cell Viability	Ref.
$NaYF_4$:Yb,Er/$NaGdF_4$ core-shell nanoparticles	33 nm (diameter) × 40 nm (length)	metal-oleate complex reduction with NaOH in methanol	980	N/A	U87MG glioblastoma cells	approx. 55%	[48]
Fe_3O_4/MnO_2-doped upconversion NPs functionalized with black phosphorous	0.31 nm for UCNPs; 50–100 nm black phosphorous	hydrothermal synthesis	808	2 W/cm^2	HeLa cells	0%	[49]

2.4. Other Metallic Nanoparticles

Other metallic nanoparticles were also used in conjugation with chlorins for biomedical purposes. Bharathiraja et al. designed nanoparticles based on copper sulfide and Ce6 for photodynamic and photothermal therapy [50]. Copper sulfide nanoparticles provided high near-infrared (NIR) absorption and hyperthermic properties. Moreover, the authors noted that a high-amplitude photoacoustic signal allows for cancer cell visualization in photoacoustic tomography (PAT) imaging. Copper sulfide nanoparticles were conjugated with Ce6 using polyethyleneimine (PEI) linker (Figure 8). The obtained nanoparticles were stable in the physiological solution for three months. In the experiment with diphenylisobenzofuran (DPBF), the authors confirmed the formation of singlet oxygen under irradiation with light at 670 nm. The conjugation of Ce6 with CuS nanoparticles was profitable for many reasons. It allowed to increase the generation of singlet oxygen and stimulated the rise of the temperature up to 53 °C (after the exposure of 200 µg/mL nanoparticles to the light at 808 nm with a power density of 2 W/cm^2 for 10 min). It is also worth noting that without irradiation, high biocompatibility of particles with cells was observed with a 92.5% survival rate. Simultaneously, the authors noted the synergistic cytotoxic activity effects related to the photothermal therapy after particle excitation with light at 808 nm and PDT when light excitation with light at 670 nm was applied. Combined photodynamic and photothermal therapy with 200 µg/mL CuS-Ce6 nanoparticles induced 84% death of MDA-MB-231 cells. However, separately performed therapies caused 55% and 41% death, respectively [50].

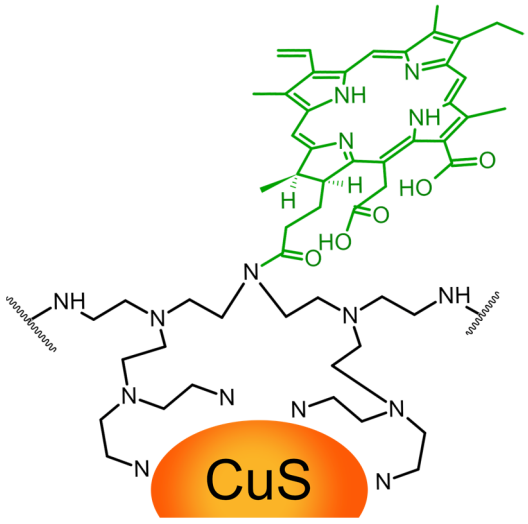


Figure 8. Chemical structure of the CuS nanoparticle (orange) surfaces, which were modified with polyethyleneimine (black) and Ce6 (green) [50].

Liu et al. also used PEI in fabricated hollow Pd nanospheres linked with Ce6 for cancer treatment using PDT/PTT [51]. The obtained nano agent, after excitation at 808 nm, effectively converted light energy into heat with a conversion efficiency η equal to 70%. Moreover, it also produced singlet oxygen under 660 nm irradiation. The nanoagent in the in vitro experiment with HeLa cells in the dark phase revealed good biocompatibility up to the concentration of 100 µg/mL. Simultaneous irradiation of nanospheres with light at wavelengths of 660 nm and 808 nm with the power of 0.5 and 2 W/cm^2, respectively, caused the death of 86% HeLa cells in the culture population. Irradiation of the nanoagent with light at 660 nm or 808 nm only gave a partial response [51].

The ternary quantum dots were proposed by Chen et al., who obtained nanorods with the core based on Cu-In-S (CIS) to which HA–polyanionic glycosaminoglycan and a Ce6 PS were covalently attached [52]. The CIS core provided photothermal properties, whereas the HA–polyglycosaminoglycan was responsible for the solubility improvement of the particles in the water environment. Moreover, this component facilitated specific binding to the cluster determinant 44 (CD44) receptors overexpressed in many cancer cells. The obtained nanoparticles of 94 nm in diameter absorbed light in the range from 400 to 1400 nm. The authors confirmed singlet oxygen formation upon nanoparticle irradiation with light at 671 nm and a photothermal effect upon irradiation with light at 808 nm. Moreover, the particles revealed high photothermal stability. The biocompatibilities were noted in the experiments in vitro with CD44-overexpressing cancer B16F1 cells and with CD44-deficient HeLa cells. Moreover, in an in vivo experiment with zebrafish embryos, no influence of nanoparticles on development was observed. In the assessment of photodynamic activity, the fabricated nanoparticles at a concentration $\geq$50 ppm activated with light at 671 nm caused the death of 60% of the B16F1 cell population. A similar result was observed for photothermal therapy when particles were activated with light at 808 nm. The authors combined these methods, which led to an 80% reduction in the cancer cell population. Cellular uptake experiments indicated that the HA component interacts with the CD44 receptor and promotes the entry of nanoparticles into the cells [52].

The multifunctional ultra-small FeS_2 nanodots with a Ce6 of a diameter ca. 7 nm were obtained by Jin et al. [53]. Nanoparticles facilitated three-way tumor imaging according to photoacoustic, magnetic resonance, and fluorescence imaging protocols. Cancerous lesions can be treated by combining photothermal and photodynamic therapies. The authors obtained nanodots via FeS_2 precipitation on bovine serum albumin (BSA) and the subsequent conjugation of Ce6 with the amide coupling method. Singlet oxygen production after irradiation with light at 660 nm was confirmed, and the photothermal effect after excitation with 808 nm was noted. The authors assessed cytotoxicity and biocompatibility in dark conditions both in vitro and in vivo and did not notice any toxic effects. Additionally, the high efficacy of combined photothermal and photodynamic treatment on 4T1 murine breast cancer cells in vitro was observed. In the in vivo model, the authors noted that combining these therapeutic approaches led to the complete eradication of the tumor, whereas when PTT and PDT were used separately, only a slight response was obtained [53].

Li et al. presented another approach for cancer treatment with combined therapy [54]. In their studies, chemotherapy, photodynamic therapy, and photothermal therapy were combined together via the fabrication of nanomaterial consisting of doxorubicin and Ce6 loaded onto CuS nanoparticles. Phase change material—1-tetradecanol was used as a stabilizing and triggering agent. Under irradiation with light at 808 nm, the photothermal effect was observed, and a temperature increase up to 43 °C (100 µg/mL) was noted. This caused the ablation of the tumor and melting of 1-tetradecanol, accompanied by the release of doxorubicin and Ce6. Furthermore, a light at 660 nm was provided to turn on the photodynamic process. In vitro studies indicated high activity of the nanomaterial against 4T1 cancer cells. Combined irradiation with light at 808 nm and 660 nm reduced cell viability significantly (ca. 1% cells left), whereas nanoparticles irradiated only with 660 nm, due to the absence of free Ce6, revealed no activity. Doxorubicin and Ce6 were released and accumulated in the nuclei and the cytoplasm, respectively. In vivo trials

were performed on BALB/c nude mouse models bearing 4T1 tumors. The obtained nanodrug was administrated intravenously and accumulated selectively in the tumor within 24 h. The treatment was performed with the same optical parameters adjusted to in vitro studies—irradiation with 808 nm prior to 660 nm. The vital signs of mice were monitored, and similar to that in in vitro experiments, the high biocompatibility of light-unaffected nanoparticles was noticed. Interestingly, the authors observed a reduction in the tumor volume by about 80% with a single treatment cycle. The performed in vitro and in vivo experiments indicated a high level of cancer cell death based on the apoptosis pathway [54].

In addition, other metals can be used as metallic nanoplatforms to develop multifunctional nanoagents. Liu et al. used MoS_2 two-dimensional nanosheets as a delivery platform for Ce6 [55]. Firstly, MoS_2 was exfoliated chemically to obtain the binding side for lipoic acid-terminated polyethylene glycol. Nanosheets bearing PEG chains were conjugated to the photosensitizer via physical adsorption with a loading capacity of ca. 30% (Ce6:MoS_2 weight ratio). Nanoplatforms loaded with Ce6 did not emit any fluorescence, but their singlet oxygen-generation ability was slightly lower than that of unbound Ce6. The authors performed experiments concerning the activity of MoS_2-PEG/Ce6 against 4T1 cancer cells using both in vitro and in vivo models. They concluded that the irradiation of cells with light at 808 nm produced a photothermal effect and also enhanced the photodynamic therapy effect (triggered at 660 nm). The MoS_2 nanoparticles irradiated with NIR light generated a temperature increase to ca. 43 °C, which also improved the cellular uptake of Ce6 molecules. High cellular uptake was assessed by the more intense intracellular fluorescence produced by Ce6 bound to the MoS_2-PEG platform compared to Ce6 alone. In the in vivo trials, no adverse effect was observed after the intravenous injection of MoS_2-PEG/Ce6. Moreover, significant tumor growth inhibition was noted under combined PTT and PDT treatment [55].

Bismuth sulfide nanostar-based nanoparticles were developed by Sun et al. [56]. The authors functionalized Bi_2S_3 nanospheres with PEG to form nanostars. A highly porous star structure was functionalized with doxorubicin for chemotherapy and Ce6 for photodynamic therapy, and subsequently, the release of both molecules was evaluated. The authors found that doxorubicin can be released from nanostars in two ways: (*i*) after the decrease in pH (low pH is present in cancer tissues) and (*ii*) upon light activation. The anticancer potential of the obtained nanomaterial was assessed in vitro using HeLa and 4T1 cancer cell lines. Efficient uptake of 97.4% of nanoparticles inside both HeLa and 4T1 cell lines after 6 h of incubation was detected. The authors also estimated biocompatibility. Nanoparticles up to the concentration of 200 μg/mL were incubated with HUVECs and with L929 mouse fibroblasts. Above 80% cell viability was noted, which suggests acceptable biocompatibility. Intracellular ROS production was confirmed with the DCFH-DA assay. In the in vitro experiments, the decrease in cancer cell viability (HeLa and 4T1) as a result of PTT/PDT/chemotherapy combined treatment was observed. Moreover, significant mitochondrial defects were observed with nanoparticles as a result of PTT/PDT treatment, as well as a prolonged body circulation half-time in comparison to that with doxorubicin only, which resulted in a higher tumor uptake rate. In the in vivo model, BALB/c mice bearing 4T1 tumors were used. The experiments in vivo proved that nanostars caused low systemic toxicity and organ damage. In these studies, the high potential of studied nanoparticles for computed tomography and fluorescence imaging, as well as the remarkable regression of the tumor, was also observed [56].

Lu et al. presented nanosheets consisting of Hf and 5,15-di(*p*-methylbenzoato)chlorin (Me_2DBC) as a linker for colon cancer photodynamic therapy [57]. The obtained nanoparticles revealed 11-fold higher light absorption in the Q band range when compared to that with the porphyrin analog and produced singlet oxygen more efficiently. Their photodynamic activity potential was assessed using in vitro and in vivo models with murine (CT26 cells) and human (HT29 cells) colorectal cancers. In these studies, excitation light at a 640 nm wavelength and a dose of 90 J/cm^2 for in vitro experiments were applied, whereas

90 and 180 J/cm^2 were used for in vivo tests. The photoactivities of chlorin and porphyrin only, as well as the obtained nanosheets conjugated with chlorin and with porphyrin, were studied. The highest potential with IC_{50} values equal to 5.1 and 6.0 μM for CT29 and HT29 cells, respectively, was observed after the use of chlorin-bearing nanosheets. Similarly, in the trials based on subcutaneous flank tumor mouse models of CT29 and HT29, the chlorin-based nanosheets presented the highest activity and caused significant tumor regression [57].

Liu et al. designed a multifunctional nanoparticle system for PDT and PTT, allowing for an increase in the partial concentration of molecular oxygen within tumor tissue [58]. It is well-known that endogenous hydrogen peroxide is present in the tumor at a reasonable concentration of up to 10^{-3} M, whereas molecular oxygen is present at a low level, causing hypoxia [59]. Therefore, the platinum nanoparticles responsible for the conversion of H_2O_2 to molecular O_2 were introduced to the bioactive material. Thanks to the production of oxygen atoms within cancerous tissue, Ce6 formed singlet oxygen efficiently. Platinum nanoparticles were encapsulated in UiO-66-NH_2—an organic framework formed by $[Zr_6O_4(OH)_4]$ clusters with 1,4-benzodicarboxy acid spacers, which was also coated with a porous gold nanoshell. Gold was responsible for the photothermal effect, and irradiation with NIR light at 808 nm and the power of 2 W/cm^2 produced heat up to 71.1 °C. The authors proved the catalytic properties of the nanoagent in the experiment with H_2O_2 decomposition, where 98.7% decomposition of this compound was noted after 3 h. The biological activity of nanoparticles was assessed in vitro using MCF-7 cells. The high biocompatibility (in dark conditions) and higher activity with combined therapies—photodynamic and photothermal—were reported in comparison to those with PDT and PTT applied separately. The high potential of the proposed approach was confirmed in the in vivo trial performed on MCF-7 tumor-bearing mice. An excellent result was noted for mice treated with combined therapy [58].

Youssef et al. reported the synthesis of TiO_2 and SiO_2-based nanoparticles bearing Ce6 [60]. Firstly, the TiO_2 or SiO_2 nanoparticle core was covered with (3-aminopropyl)triethoxysilane, as well as a shell to which Ce6 was attached via an amide bond. Titanium oxide nanoparticles revealed higher biological activity with high ROS generation, especially OH· radicals, which was confirmed under light irradiation of the U87 glioblastoma cell line inside. Despite the high anticancer activity, significant activity in dark conditions was also noticed [60].

The mesoporous silicon nanoparticles (MSNs) loaded with Ce6, L-buthionine sulfoximine (BSO), and further with cisplatin were recently proposed by Xu et al. as a multifunctional antitumor agents, combining PDT with classic chemotherapy [61]. The in vitro and in vivo experiments based on A549/DDP tumor-bearing nude mice using nanoparticles revealed that all components were released separately under acidic conditions in tumor tissue, leading to a tumor inhibitory rate (vs. saline) of 73.8%. The data described in Section 2.4 are summarized in Table 4.

Table 4. A summary of the data presented in Section 2.4.

Type of NPs	Size of NPs	Preparation Method	Wavelength [nm]	Light Dose/Light Power	Cell Type	Cell Viability	Ref.
CuS	6.5 nm	chemical reduction of copper(I) chloride in octadecene (ODE)	670 and 808	100 mW/cm^2 for 670 nm and 2 W/cm^2 for 808 nm	MDA-MB-231 breast cancer cells	16%	[50]
Pd nanospheres	90 nm	hydrothermal synthesis	660 and 808	0.5 W/cm^2 for 660 nm and 2 W/cm^2 for 808 nm	HeLa cells	14%	[51]

Table 4. *Cont.*

Type of NPs	Size of NPs	Preparation Method	Wavelength [nm]	Light Dose/Light Power	Cell Type	Cell Viability	Ref.
Cu-In-S quantum dots	30 nm	solvothermal method	671 and 808	1 W/cm^2 for 671 nm and 2 W/cm^2 for 808 nm	B16F1 mouse melanoma cells	<15%	[52]
FeS_2 nanodots	7 nm	biomineralization of $FeCl_2$	660 and 808	5 mW/cm^2 for 660 nm and 0.8 W/cm^2 for 808 nm	murine breast cancer (4T1) cells	20%	[53]
CuS	184.2 ± 4.8 nm	chemical reduction of copper(I) chloride by NaOH and further treatment with $(NH_4)_2S$	660 and 808	0.5 W/cm^2 for 660 nm and 2 W/cm^2 for 808 nm	4T1 mouse mammary tumor cell line	1.68%	[54]
MoS_2	~1 nm	exfoliation of the bulk MoS_2 with *n*-butyl lithium	660 and 808	5 mW/cm^2 for 660 nm and 0.5 W/cm^2 for 808 nm	4T1 mouse mammary tumor cell line	approx. 15%	[55]
Bi_2S_3 nanospheres	~186.2 nm	chemical reduction of $Bi(NO_3)_3$ by NaOH in the presence of HNO_3 and ethylene glycol	660 and 808	0.38 W/cm^2 for 660 nm and 2 W/cm^2 for 808 nm	HeLa cells	6.26 ± 0.21%	[56]
Hf nanosheets	100–200 nm × 3.3 − 7.5 nm	solvothermal method	640 or 650	0.1 W/cm^2 (90 J/cm^2)	CT26 cells HT29 cells	20% 25%	[57]
Pt nanoparticles in the $[Zr_6O_4(OH)_4]$ clusters	60 nm	solvothermal method (MOF) encapsulation of Pt NPs in MOF structure	670 and 808	50 mW/cm^2 for 670 nm and 1 W/cm^2 for 808 nm	human breast cancer MCF-7 cells	approx. 10%	[58]
TiO_2 or SiO_2 nanoparticles	~30 nm	silanization process of TiO_2 or SiO_2	652	4.54 mW/cm^2 (10 J/cm^2)	glioblastoma U87 cells	11%	[60]
mesoporous silicon NPs	~211.4 nm	chemical reduction of tetraethyl orthosilicate by NaOH in the presence of hexadecyl trimethyl ammonium bromide	660	100 mW/cm^2	human lung adenocarcinoma A549/DDP cells	0.3% ± 0.4%	[61]

2.5. Carbon-Based Nanomaterials

Carbon-based nanomaterials also constitute interesting nanosystems that, combined with Ce6, demonstrated good cytotoxic effects. An interesting study in this regard was performed by Fan et al., who developed efficient anti-TNBC (triple-negative breast cancer) agents based on graphene oxide quantum dots (GOQDs) [62]. Two nanosystems were fabricated. In both of them, GOQDs were coated with PLGA and conjugated with capsaicin or grafted with gamabufotalin and Ce and then coated with red blood cell–cancer hybrid membranes. In vitro cytotoxicity studies with MDA-MB-231 cells revealed cell viability at 29% after 660 nm irradiation [62].

Catalytic conversion of H_2O_2 to O_2 within the tumor was also reported by Yin et al. [63]. They coated the carbon nanotubes with cross-linked MnO_2 flakes with adsorbed Ce6. Further, the authors confirmed, in the in vitro and in vivo experiments, a high potential of the obtained nanosystem for PTT and PDT, as well as in dual fluorescence-photothermal tumor imaging [63].

A one-step hydrothermal method using p-aminobenzamide and p-aminosalicylic acid was used to prepare other carbon-based NPs—green fluorescence carbon dots conjugated with epidermal growth factor, cis-platin, and Ce6 [64]. The PS incorporated into GCDs provided the nano-assembly imaging ability and facilitated image-guided therapy. The authors used the obtained nanomaterial in the in vitro study with human esophageal

squamous cell carcinoma KYSE-150 cells, achieving 20% cell viability after laser irradiation (660 nm, 0.2 W/cm^2). Moreover, very good tumor remission was obtained in in vivo studies, especially for EGFR-bearing tumors [64]. The data described in Section 2.5 are summarized in Table 5.

Table 5. Summary of the data presented in Section 2.5.

Type of NPs	Size of NPs	Preparation Method	Wavelength [nm]	Light Dose/Light Power	Cell Type	Cell Viability	Ref.
Graphene oxide quantum dots	144.7 nm	N/A	660	0.1 W/cm^2	MDA-MB-231 breast cancer cells	29%	[62]
Carbon nanotubes with cross-linked MnO_2 flakes	113 nm	cross-linking of MnO_2 flakes on carbon nanotubes	660 and 808	40 mW/cm^2 for 670 nm and 1 W/cm^2 for 808 nm	HeLa cells	approx. 25%	[63]
Carbon dots	90.56 ± 2.07 nm for GCDs-Ce6/Pt-EGF	one-step hydrothermal method using *p*-aminobenzamide and *p*-aminosalicylic acid	660	0.5 W/cm^2	Human esophageal squamous cell carcinoma KYSE-150 cells	approx. 20%	[64]

2.6. Metal-Organic Frameworks

The metal–organic frameworks with high flexibility and porosity can be synthesized by combining metal-containing subunits (inorganic clusters) and organic linkers (carboxylates, imidazolates, and phosphonates). Such systems constitute promising drug delivery carriers, as well as theranostic agents. The MOF nanoparticles bearing Ce6 and camptothecin (Cam) for photodynamic therapy and chemotherapy as multimodal agents were presented by Liu et al. (Figure 9) [65]. Moreover, the obtained nanoplatform was attached to folic acid (FA), thus facilitating targeted delivery. The authors fabricated the nanoagent with the Ce6 derivative triggered by cathepsin B, an enzyme present mainly in cancerous cells. Ce6 linked with the peptide—a substrate for cathepsin B—did not reveal any photodynamic activities, but after cutting the peptide moiety off and releasing Ce6, the photodynamic properties were turned on. In the in vitro experiments, Liu et al. showed that the nanoagent was efficiently delivered into HeLa cells compared to that with HaCaT (immortalized human keratinocytes) cells. It is known that HeLa and many other cancer cells possess folic acid receptors, unlike non-cancerous HaCaT cells. The authors presented the targeted delivery of Ce6 into the cells, which was indicated by photosensitizer fluorescence turned on by intracellular cathepsin B. The intracellular singlet oxygen production was indicated with Singlet Oxygen Sensor Green. The cytotoxic assessment experiments showed that combined chemo- and photodynamic therapy influenced the apoptosis of 99.27% HeLa cells upon light excitation (60 J/cm^2 at 660 nm), while in the dark condition, only 35.17% of cells were eliminated. Interestingly, the same level of cancer cell death was achieved only for Ce6 MOF, loaded after 30 min of irradiation. Simultaneously, the experiments using cells without folic acid receptors were performed, and no activity was noted. In the in vivo trials, the usability of the nanoagent was tested with the HeLa tumor mouse model. The developed MOF preferentially accumulated in the tumor within 24 h after intravenous injection. In the tumor, Ce6 was triggered by cathepsin B and emitted strong fluorescence. A significantly higher decrease in the tumor volume was noted when treated with Cam-Ce6-pept-FA-MOF nanoparticles in comparison to that with Cam-FA-MOF or Ce6-FA-MOF [65].

In another study, Lu et al., synthesized a novel MOF based on *meso*-5,10,15,20-tetrakis(4-carboxyphenyl)chlorin combined with Hf^{4+} [66]. MOF was then loaded with an indoleamine 2,3-dioxygenase inhibitor. The material was tested on mice bearing CT26 and MC38 colorectal cancer tumors and was found to be effective in PDT and the immunotherapeutic treatment of metastatic tumors [66].

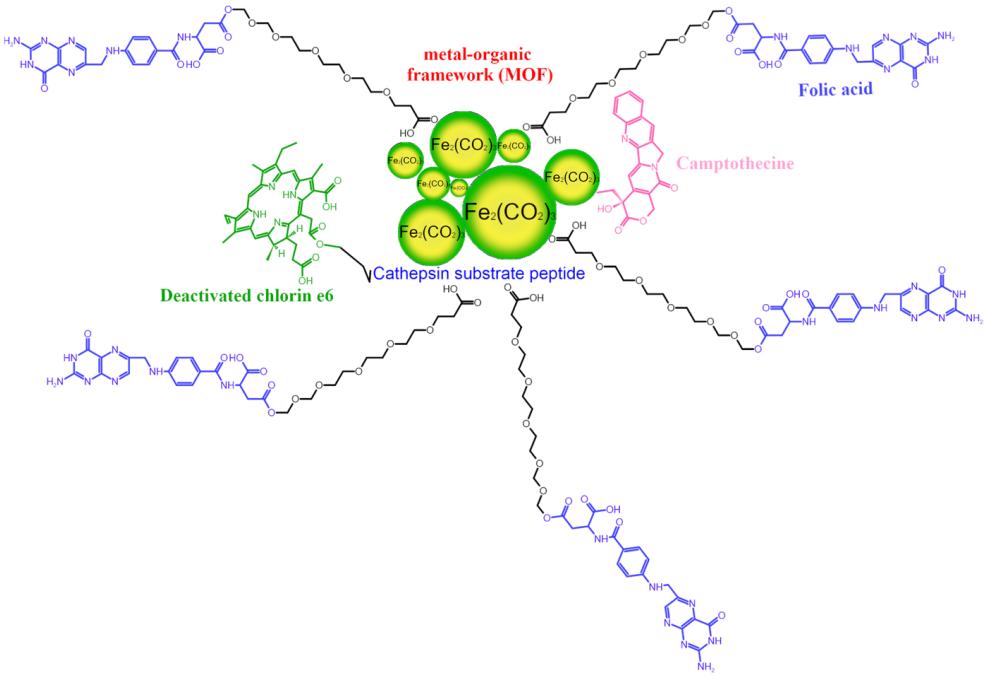


Figure 9. Chemical structure of the MOF nanoparticles bearing folic acid (blue), Ce6 (green), and camptothecin (pink) [65].

Other chlorin derivatives were also studied in the theranostic approach to cancer treatment. Zheng et al. utilized tetratopic chlorin as a PS and Hf-UiO-66 as an isomorphic analog of Zr-UiO-66 (MOF) [67]. Chlorin implemented into MOF revealed both photothermal and photodynamic activity. Interestingly, in the experiments on HepG2, HeLa, 4T1, and MCF-7 cells in vitro, it was observed that the photodynamic effect produced only ca. 30% cell death, whereas the photothermal effect induced ca. 65% death. This phenomenon was combined with the observed decrease in singlet oxygen formation mediated by a chlorin derivative introduced into the MOF structure compared to that with a free photosensitizer. In the in vivo trials, the authors proved the high biocompatibility of the obtained material. They did not note significant hemolysis (<5%). Moreover, no influence of coagulation factors and no changes in the biochemistry profile were noted. Moreover, the authors detected higher PTT/PDT treatment effectiveness when MOFs were administrated intravenously compared to direct injection into the tumor. Besides high in vivo PTT/PDT activity against the tumor, the possibility of computed tomography and photoacoustic imaging was also reported [67]. The data described in Section 2.6 are summarized in Table 6.

Table 6. Summary of the data presented in Section 2.6.

Type of NPs	Size of NPs	Preparation Method	Wavelength [nm]	Light Dose/Light Power	Cell Type	Cell Viability	Ref.
$FE_2(CO_2)_3$ MOFs	95 nm	microwave-assisted synthesis	660	100 mW/cm^2	HeLa cells	0.73%	[65]
Hf^{4+} MOFs	72.7 and 83.2 nm	solvothermal method	650	100 mW/cm^2 (90 J/cm^2)	colorectal cancer CT26 and MC38 cells	approx. 10–15%	[66]
Hf-UiO-66 MOFs	100–130 nm	solvothermal method	635	0.8 W/cm^2	HepG2 and HeLa cells	approx. 35%	[67]

2.7. Polymer-Based Nanoparticles

The use of polymers to create modern carriers for PSs is of great interest and has been the subject ofnumerous in vitro and in vivo studies. Recently, two interesting examples of Ce6-polymer conjugates were presented. Park et al. fabricated a dextran sulfate-based nano-photosensitizer selectively targeting macrophages in co-cultured 4T1 tumors/macrophages [68]. The chlorin moieties were attached to the polymer via ester-groups. In the in vitro studies with 4T1-Luc breast cancer cells, the induced tumor apoptosis was observed after 670 nm laser irradiation. Moreover, an excellent cytotoxic effect was achieved in in vivo studies with 4T1 tumor-bearing mice [68].

The other polymeric nano-sized drug delivery system consisting of Ce6 and a cathepsin B-sensitive polymer-paclitaxel prodrug was obtained by Tan et al. [69]. The enhanced cytotoxic activity of the obtained system was achieved via a two-stage light irradiation strategy using 660 nm laser irradiation. The studies performed with human bladder cancer PDX models revealed excellent tumor growth inhibition (>98%). What is more, the bioinformatics analysis showed that the combination of PDT with classic chemotherapy provided by paclitaxel led to a decrease in the pathways related to tumor progression, invasion, and metastasis (hypoxia, TGF-β, and TNF-α signaling) [69].

2.8. Bacteriochlorins

There are also examples of other structurally related chlorin macrocycles conjugated with metal nanoparticles. Pantiushenko et al. synthesized gold nanoparticles bound via sulfur with bacteriochlorophyll for tumor visualization in optical imaging [70]. The authors studied the potential of the nanoagent for imaging using an in vivo rat sarcoma M-1 model. They reported the highest fluorescence signal within tumor tissue 3 h after administration. In other studies, Zhang et al. developed MOFs based on Hf-bearing bactriochlorin (DBBC-**di**benzoate**b**acterio**c**hlorin) [71]. They obtained nanosheet DBBC-UiO, and the designed MOFs predominantly formed superoxide anion radical $O_2^{\cdot -}$, as well as singlet oxygen. The high anticancer activity of these systems was confirmed in in vitro and in vivo experiments. In the in vitro study on MCF-7 cancer cell cultures, after the introduction and irradiation of nanoparticles, over 90% of dead cells were detected, while in vivo, tumor tissue was diminished after 15 days. Simultaneously, the authors studied the biocompatibility of the obtained structure, and no impact of the nanostructures on cell viability was noted in in vitro experiments. Moreover, during the in vivo studies, no biochemistry parameter deviations or organ destruction were observed [71].

3. Conclusions

In the presented review, numerous types of conjugates consisting of diverse metallic nanoparticles with Ce6 and its derivatives were described, and the studies clearly indicate a significant advantage of iron oxide and gold nanoparticles. In addition, many variants of binding between porphyrinoids and nanoparticles were presented, including electrostatic interactions, covalent linking, and encapsulation. Considering the above-described data, one can conclude that there are several advantages of conjugating metallic nanoparticles with chlorin-type photosensitizers. Some of the advantages are as follows: (*i*) the conjugates usually facilitate the performance of in vitro or in vivo multimodal therapy, where PDT can be combined with the photo-/magnetothermal therapy or with the classic chemotherapy driven by doxorubicin or cisplatin, (*ii*) the conjugation of the photosensitizer with metallic nanoparticles can enhance reactive oxygen species formation by catalyzing the decomposition of H_2O_2 and an increase of the oxygen concentration, and (*iii*) apart from therapeutic applications, the obtained conjugates can be utilized in cancer diagnostics based on the intense fluorescence of chlorin macrocycle (PDD) and/or amplification of the MRI intensity.

In general, the use of nanoparticles as carriers enables the attachment of additional targeting molecules while simplifying the synthetic procedures, most notably the purification step. Additionally, nanoparticles functionalized with targeting moieties increase the selectivity and therapeutic efficacy of the systems in in vivo studies, allowing for the effective

combination of different therapies. It is also worth noting that in combined therapy, more than one trigger for ROS or cytotoxicity is used, which leads to higher activation yields and better therapeutic results. A combination of metallic nanoparticles and porphyrinoids usually increases singlet oxygen generation. Moreover, metallic nanoparticles open access to imaging alongside increased therapeutic outcomes. However, despite the abovementioned advantages of these conjugates, some risks can also accompany the usage of functionalized nanoparticles in cancer treatment. There are some biosafety concerns regarding NP metabolism, degradation, and accumulation. For example, the passive absorption of nanoparticles can cause acute hypersensitivity in healthy tissue since they cannot be distinguished from neoplastic cells [72]. To avoid the negative impact of metallic nanoparticles on healthy tissue in PDT, carrier-free nanomedicines are constructed via the nano-assembly of photosensitizing compounds in simple procedures, allowing for the delivery of dual or multi-components for combination therapy PDT/PTT/chemotherapy [73].

Author Contributions: Conceptualization, T.K., T.G. and L.S.; investigation, T.K., A.G.-S., D.T.M. and M.M.; resources, M.M. and L.S.; writing—original draft preparation, T.K., M.M. and L.S.; writing—review and editing, E.G., T.G. and L.S.; visualization, L.S.; supervision, T.G. and L.S.; project administration, T.G.; funding acquisition, T.G. All authors have read and agreed to the published version of the manuscript.

Funding: The authors acknowledge the funding provided by the National Science Centre, Poland, under Grant No. 2020/39/O/NZ7/00351.

Institutional Review Board Statement: Not applicable.

Informed Consent Statement: Not applicable.

Data Availability Statement: Not applicable.

Acknowledgments: The authors would like to thank Beata Kwiatkowska and Rita Kuba for their support.

Conflicts of Interest: The authors declare no conflict of interest.

References

1. Yoon, I.; Li, J.Z.; Shim, Y.K. Advance in Photosensitizers and Light Delivery for Photodynamic Therapy. *Clin. Endosc.* **2013**, *46*, 7–23. [CrossRef] [PubMed]
2. Borbas, K.E.; Chandrashaker, V.; Muthiah, C.; Hooi, L.K.; Holten, D.; Lindsey, J.S. Design, Synthesis, and Photophysical Characterization of Water-Soluble Chlorins. *J. Org. Chem.* **2008**, *73*, 3145–3158. [CrossRef] [PubMed]
3. Allison, R.R.; Moghissi, K. Photodynamic Therapy (PDT): PDT Mechanisms. *Clin. Endosc.* **2013**, *46*, 24–29. [CrossRef]
4. Dąbrowski, J.M.; Arnaut, L.G. Photodynamic Therapy (PDT) of Cancer: From Local to Systemic Treatment. *Photochem. Photobiol. Sci.* **2015**, *14*, 1765–1780. [CrossRef] [PubMed]
5. Costa, D.C.S.; Gomes, M.C.; Faustino, M.A.F.; Neves, M.G.P.M.S.; Cunha, Â.; Cavaleiro, J.A.S.; Almeida, A.; Tomé, J.P.C. Comparative Photodynamic Inactivation of Antibiotic Resistant Bacteria by First and Second Generation Cationic Photosensitizers. *Photochem. Photobiol. Sci.* **2012**, *11*, 1905–1913. [CrossRef]
6. Yue, L.; Zheng, M.; Khan, I.M.; Wang, Z. Chlorin E6 Conjugated Chitosan as an Efficient Photoantimicrobial Agent. *Int. J. Biol. Macromol.* **2021**, *183*, 1309–1316. [CrossRef]
7. Glowacka-Sobotta, A.; Ziental, D.; Sobotta, L. Chapter 12. Porphyrinoids Used for Photodynamic Inactivation against Bacteria. In *Applications of Porphyrinoids as Functional Materials*; Lang, H., Rueffer, T., Eds.; Smart Materials; Royal Society of Chemistry: Cambridge, UK, 2021; pp. 352–404. ISBN 978-1-83916-188-9.
8. Nishie, H.; Kataoka, H.; Yano, S.; Yamaguchi, H.; Nomoto, A.; Tanaka, M.; Kato, A.; Shimura, T.; Mizoshita, T.; Kubota, E.; et al. Excellent Antitumor Effects for Gastrointestinal Cancers Using Photodynamic Therapy with a Novel Glucose Conjugated Chlorin E6. *Biochem. Biophys. Res. Commun.* **2018**, *496*, 1204–1209. [CrossRef]
9. Martynenko, I.V.; Kuznetsova, V.A.; Orlova, O.; Kanaev, P.A.; Maslov, V.G.; Loudon, A.; Zaharov, V.; Parfenov, P.; Gun'Ko, Y.K.; Baranov, A.V.; et al. Chlorin E6-ZnSe/ZnS Quantum Dots Based System as Reagent for Photodynamic Therapy. *Nanotechnology* **2015**, *26*, 55102. [CrossRef]
10. Alea-Reyes, M.E.; Soriano, J.; Mora-Espí, I.; Rodrigues, M.; Russell, D.A.; Barrios, L.; Pérez-García, L. Amphiphilic Gemini Pyridinium-Mediated Incorporation of Zn(II)Meso-Tetrakis(4-Carboxyphenyl)Porphyrin into Water-Soluble Gold Nanoparticles for Photodynamic Therapy. *Colloids Surf. B Biointerfaces* **2017**, *158*, 602–609. [CrossRef]
11. Homayoni, H.; Ma, L.; Zhang, J.; Sahi, S.K.; Rashidi, L.H.; Bui, B.; Chen, W. Synthesis and Conjugation of $Sr_2MgSi_2O_7$:Eu^{2+}, Dy^{3+} Water Soluble Afterglow Nanoparticles for Photodynamic Activation. *Photodiagnosis Photodyn. Ther.* **2016**, *16*, 90–99. [CrossRef]

12. Alea-Reyes, M.E.; Rodrigues, M.; Serrà, A.; Mora, M.; Sagristá, M.L.; González, A.; Durán, S.; Duch, M.; Plaza, J.A.; Vallés, E.; et al. Nanostructured Materials for Photodynamic Therapy: Synthesis, Characterization and in Vitro Activity. *RSC Adv.* **2017**, *7*, 16963–16976. [CrossRef]
13. Ferreira, D.C.; Monteiro, C.S.; Chaves, C.R.; Sáfar, G.A.M.; Moreira, R.L.; Pinheiro, M.V.B.; Martins, D.C.S.; Ladeira, L.O.; Krambrock, K. Hybrid Systems Based on Gold Nanostructures and Porphyrins as Promising Photosensitizers for Photodynamic Therapy. *Colloids Surf. B Biointerfaces* **2017**, *150*, 297–307. [CrossRef] [PubMed]
14. Chen, R.J.; Chen, P.C.; Prasannan, A.; Vinayagam, J.; Huang, C.C.; Chou, P.Y.; Weng, C.C.; Tsai, H.C.; Lin, S.Y. Formation of Gold Decorated Porphyrin Nanoparticles and Evaluation of Their Photothermal and Photodynamic Activity. *Mater. Sci. Eng. C* **2016**, *63*, 678–685. [CrossRef]
15. Koczorowski, T.; Glowacka-Sobotta, A.; Sysak, S.; Mlynarczyk, D.T.; Lesyk, R.; Goslinski, T.; Sobotta, L. BODIPY-Based Nanomaterials-Sensing and Biomedical Applications. *Appl. Sci. Switz.* **2022**, 7815. [CrossRef]
16. Di Corato, R.; Béalle, G.; Kolosnjaj-Tabi, J.; Espinosa, A.; Clément, O.; Silva, A.K.A.; Ménager, C.; Wilhelm, C. Combining Magnetic Hyperthermia and Photodynamic Therapy for Tumor Ablation with Photoresponsive Magnetic Liposomes. *ACS Nano* **2015**, *9*, 2904–2916. [CrossRef] [PubMed]
17. Huang, P.; Li, Z.; Lin, J.; Yang, D.; Gao, G.; Xu, C.; Bao, L.; Zhang, C.; Wang, K.; Song, H.; et al. Photosensitizer-Conjugated Magnetic Nanoparticles for in Vivo Simultaneous Magnetofluorescent Imaging and Targeting Therapy. *Biomaterials* **2011**, *32*, 3447–3458. [CrossRef]
18. Amirshaghaghi, A.; Yan, L.; Miller, J.; Daniel, Y.; Stein, J.M.; Busch, T.M.; Cheng, Z.; Tsourkas, A. Chlorin E6-Coated Superparamagnetic Iron Oxide Nanoparticle (SPION) Nanoclusters as a Theranostic Agent for Dual-Mode Imaging and Photodynamic Therapy. *Sci. Rep.* **2019**, *9*, 1–9. [CrossRef]
19. Yang, H.Y.; Fu, Y.; Li, Y.; Jang, M.S.; Lee, J.H.; Lee, D.S. Polymer Ligand-Assisted Fabrication of Multifunctional and Redox-Responsive Self-Assembled Magnetic Nanoclusters for Bimodal Imaging and Cancer Treatment. *J. Mater. Chem. B* **2018**, *6*, 5562–5569. [CrossRef]
20. Yu, T.T.; Peng, X.C.; Wang, M.F.; Han, N.; Xu, H.Z.; Li, Q.R.; Li, L.G.; Xu, X.; Ma, Q.L.; Liu, B.; et al. Harnessing Chlorin E6 Loaded by Functionalized Iron Oxide Nanoparticles Linked with Glucose for Target Photodynamic Therapy and Improving of the Immunogenicity of Lung Cancer. *J. Cancer Res. Clin. Oncol.* **2022**, *148*, 867–879. [CrossRef]
21. McCarthy, J.R.; Korngold, E.; Weissleder, R.; Jaffer, F.A. A Light-Activated Theranostic Nanoagent for Targeted Macrophage Ablation in Inflammatory Atherosclerosis. *Small* **2010**, *6*, 2041–2049. [CrossRef]
22. Işıklan, N.; Hussien, N.A.; Türk, M. Multifunctional Aptamer-Conjugated Magnetite Graphene Oxide/Chlorin E6 Nanocomposite for Combined Chemo-Phototherapy. *Colloids Surf. Physicochem. Eng. Asp.* **2022**, *645*. [CrossRef]
23. Hu, H.; Li, R.; Huang, P.; Mo, Z.; Xu, Q.; Hu, T.; Yao, S.; Dai, X.; Xu, Z. BSA-Coated β-FeOOH Nanoparticles Efficiently Deliver the Photosensitizer Chlorin E6 for Synergistic Anticancer PDT/CDT. *Colloids Surf. B Biointerfaces* **2023**, *222*, 1–10. [CrossRef]
24. Ling, D.; Park, W.; Park, S.J.; Lu, Y.; Kim, K.S.; Hackett, M.J.; Kim, B.H.; Yim, H.; Jeon, Y.S.; Na, K.; et al. Multifunctional Tumor PH-Sensitive Self-Assembled Nanoparticles for Bimodal Imaging and Treatment of Resistant Heterogeneous Tumors. *J. Am. Chem. Soc.* **2014**, *136*, 5647–5655. [CrossRef] [PubMed]
25. Xu, Z.; Chen, J.; Li, Y.; Hu, T.; Fan, L.; Xi, J.; Han, J.; Guo, R. Yolk-Shell Fe3O4@Carbon@Platinum-Chlorin E6 Nanozyme for MRI-Assisted Synergistic Catalytic-Photodynamic-Photothermal Tumor Therapy. *J. Colloid Interface Sci.* **2022**, *628*, 1033–1043. [CrossRef]
26. Magro, M.; Bramuzzo, S.; Baratella, D.; Ugolotti, J.; Zoppellaro, G.; Chemello, G.; Olivotto, I.; Ballarin, C.; Radaelli, G.; Arcaro, B.; et al. Self-Assembly of Chlorin-E6 on γ-Fe 2 O 3 Nanoparticles: Application for Larvicidal Activity against Aedes Aegypti. *J. Photochem. Photobiol. B* **2019**, *194*, 21–31. [CrossRef]
27. Zhang, H.; Li, H.; Fan, H.; Yan, J.; Meng, D.; Hou, S.; Ji, Y.; Wu, X. Formation of Plasmon Quenching Dips Greatly Enhances 1O2 Generation in a Chlorin E6–Gold Nanorod Coupled System. *Nano Res.* **2018**, *11*, 1456–1469. [CrossRef]
28. Tian, S.; He, J.; Lyu, D.; Li, S.; Xu, Q.H. Aggregation Enhanced Photoactivity of Photosensitizer Conjugated Metal Nanoparticles for Multimodal Imaging and Synergistic Phototherapy below Skin Tolerance Threshold. *Nano Today* **2022**, *45*, 101534. [CrossRef]
29. Gao, F.; Sun, M.; Xu, L.; Liu, L.; Kuang, H.; Xu, C. Biocompatible Cup-Shaped Nanocrystal with Ultrahigh Photothermal Efficiency as Tumor Therapeutic Agent. *Adv. Funct. Mater.* **2017**, *27*, 1–6. [CrossRef]
30. Wu, F.; Liu, Y.; Wu, Y.; Song, D.; Qian, J.; Zhu, B. Chlorin E6 and Polydopamine Modified Gold Nanoflowers for Combined Photothermal and Photodynamic Therapy. *J. Mater. Chem. B* **2020**, *8*, 2128–2138. [CrossRef]
31. Gil-Tomás, J.; Dekker, L.; Narband, N.; Parkin, I.P.; Nair, S.P.; Street, C.; Wilson, M. Lethal Photosensitisation of Bacteria Using a Tin Chlorin E6-Glutathione-Gold Nanoparticle Conjugate. *J. Mater. Chem.* **2011**, *21*, 4189–4196. [CrossRef]
32. Vieira, L.; Castilho, M.L.; Ferreira, I.; Ferreira-Strixino, J.; Hewitt, K.C.; Raniero, L. Synthesis and Characterization of Gold Nanostructured Chorin E6 for Photodynamic Therapy. *Photodiagnosis Photodyn. Ther.* **2017**, *18*, 6–11. [CrossRef] [PubMed]
33. Sun, M.; Xu, L.; Ma, W.; Wu, X.; Kuang, H.; Wang, L.; Xu, C. Hierarchical Plasmonic Nanorods and Upconversion Core-Satellite Nanoassemblies for Multimodal Imaging-Guided Combination Phototherapy. *Adv. Mater.* **2016**, *28*, 898–904. [CrossRef] [PubMed]
34. Castilho, M.L.; Jesus, V.P.S.; Vieira, P.F.A.; Hewitt, K.C.; Raniero, L. Chlorin E6-EGF Conjugated Gold Nanoparticles as a Nanomedicine Based Therapeutic Agent for Triple Negative Breast Cancer. *Photodiagnosis Photodyn. Ther.* **2021**, *33*, 102186. [CrossRef] [PubMed]

35. Yeo, E.L.L.; Cheah, J.U.J.; Neo, D.J.H.; Goh, W.I.; Kanchanawong, P.; Soo, K.C.; Thong, P.S.P.; Kah, J.C.Y. Exploiting the Protein Corona around Gold Nanorods for Low-Dose Combined Photothermal and Photodynamic Therapy. *J. Mater. Chem. B* **2017**, *5*, 254–268. [CrossRef]
36. Huang, P.; Lin, J.; Wang, S.; Zhou, Z.; Li, Z.; Wang, Z.; Zhang, C.; Yue, X.; Niu, G.; Yang, M.; et al. Photosensitizer-Conjugated Silica-Coated Gold Nanoclusters for Fluorescence Imaging-Guided Photodynamic Therapy. *Biomaterials* **2013**, *34*, 4643–4654. [CrossRef] [PubMed]
37. Yu, M.; Guo, F.; Wang, J.; Tan, F.; Li, N. Photosensitizer-Loaded PH-Responsive Hollow Gold Nanospheres for Single Light-Induced Photothermal/Photodynamic Therapy. *ACS Appl. Mater. Interfaces* **2015**, *7*, 17592–17597. [CrossRef]
38. Yu, M.; Guo, F.; Wang, J.; Tan, F.; Li, N. A PH-Driven and Photoresponsive Nanocarrier: Remotely-Controlled by near-Infrared Light for Stepwise Antitumor Treatment. *Biomaterials* **2016**, *79*, 25–35. [CrossRef]
39. Haimov, E.; Weitman, H.; Polani, S.; Schori, H.; Zitoun, D.; Shefi, O. Meso-Tetrahydroxyphenylchlorin-Conjugated Gold Nanoparticles as a Tool to Improve Photodynamic Therapy. *ACS Appl. Mater. Interfaces* **2018**, *10*, 2319–2327. [CrossRef]
40. Li, B.; Fu, Y.; Xie, M.; Feng, L.; Niu, X.; Que, L.; You, Z. Gold-Based Nanoparticles Realize Photothermal and Photodynamic Synergistic Treatment of Liver Cancer and Improve the Anaerobic Tumor Microenvironment under near-Infrared Light. *Front. Bioeng. Biotechnol.* **2022**, *10*, 1–12. [CrossRef]
41. Magalhães, J.A.; Fernandes, A.U.; Junqueira, H.C.; Nines, B.C.; Cursino, T.A.F.; Formaggio, D.M.D.; Baptista, M.S.; Tada, D.B. Bimetallic Nanoparticles Enhance Photoactivity of Conjugated Photosensitizer. *Nanotechnology* **2020**, *31*, 095102. [CrossRef]
42. Zhang, C.; Li, C.; Liu, Y.; Zhang, J.; Bao, C.; Liang, S.; Wang, Q.; Yang, Y.; Fu, H.; Wang, K.; et al. Gold Nanoclusters-Based Nanoprobes for Simultaneous Fluorescence Imaging and Targeted Photodynamic Therapy with Superior Penetration and Retention Behavior in Tumors. *Adv. Funct. Mater.* **2015**, *25*, 1314–1325. [CrossRef]
43. Zhang, R.Y.; Cheng, K.; Xuan, Y.; Yang, X.Q.; An, J.; Hu, Y.G.; Liu, B.; Zhao, Y. Di A PH/Ultrasonic Dual-Response Step-Targeting Enterosoluble Granule for Combined Sonodynamic-Chemotherapy Guided: Via Gastrointestinal Tract Imaging in Orthotopic Colorectal Cancer. *Nanoscale* **2021**, *13*, 4278–4294. [CrossRef] [PubMed]
44. Wysocki, M.; Czarczynska-Goslinska, B.; Ziental, D.; Michalak, M.; Güzel, E.; Sobotta, L. Excited State and Reactive Oxygen Species against Cancer and Pathogens: A Review on Sonodynamic and Sono-Photodynamic Therapy. *ChemMedChem* **2022**, *17*. [CrossRef]
45. Wijesiri, N.; Ozkaya-Ahmadov, T.; Wang, P.; Zhang, J.; Tang, H.; Yu, X.; Ayres, N.; Zhang, P. Photodynamic Inactivation of Multidrug-Resistant Staphylococcus Aureus Using Hybrid Photosensitizers Based on Amphiphilic Block Copolymer-Functionalized Gold Nanoparticles. *ACS Omega* **2017**, *2*, 5364–5369. [CrossRef] [PubMed]
46. Wu, L.; Wang, J.; Yin, M.; Ren, J.; Miyoshi, D.; Sugimoto, N.; Qu, X. Reduced Graphene Oxide Upconversion Nanoparticle Hybrid for Electrochemiluminescent Sensing of a Prognostic Indicator in Early-Stage Cancer. *Small* **2014**, *10*, 330–336. [CrossRef]
47. Wang, C.; Cheng, L.; Liu, Z. Drug Delivery with Upconversion Nanoparticles for Multi-Functional Targeted Cancer Cell Imaging and Therapy. *Biomaterials* **2011**, *32*, 1110–1120. [CrossRef]
48. Park, Y.I.; Kim, H.M.; Kim, J.H.; Moon, K.C.; Yoo, B.; Lee, K.T.; Lee, N.; Choi, Y.; Park, W.; Ling, D.; et al. Theranostic Probe Based on Lanthanide-Doped Nanoparticles for Simultaneous in Vivo Dual-Modal Imaging and Photodynamic Therapy. *Adv. Mater.* **2012**, *24*, 5755–5761. [CrossRef]
49. Zhang, Q.; Wang, W.; Zhang, M.; Wu, F.; Zheng, T.; Sheng, B.; Liu, Y.; Shen, J.; Zhou, N.; Sun, Y. A Theranostic Nanocomposite with Integrated Black Phosphorus Nanosheet, Fe_3O_4@MnO_2-Doped Upconversion Nanoparticles and Chlorin for Simultaneous Multimodal Imaging, Highly Efficient Photodynamic and Photothermal Therapy. *Chem. Eng. J.* **2020**, *391*, 123525. [CrossRef]
50. Bharathiraja, S.; Manivasagan, P.; Moorthy, M.S.; Bui, N.Q.; Lee, K.D.; Oh, J. Chlorin E6 Conjugated Copper Sulfide Nanoparticles for Photodynamic Combined Photothermal Therapy. *Photodiagnosis Photodyn. Ther.* **2017**, *19*, 128–134. [CrossRef]
51. Liu, Y.; Ding, L.; Wang, D.; Lin, M.; Sun, H.; Zhang, H.; Sun, H.; Yang, B. Hollow Pd Nanospheres Conjugated with Ce6 to Simultaneously Realize Photodynamic and Photothermal Therapy. *ACS Appl. Bio Mater.* **2018**, *1*, 1102–1108. [CrossRef] [PubMed]
52. Chen, S.H.; Huang, W.W.; Dehvari, K.; Ling, Y.C.; Ghule, A.V.; Tsai, S.L.; Chang, J.Y. Photosensitizer–Conjugated Cu-In-S Heterostructured Nanorods for Cancer Targeted Photothermal/Photodynamic Synergistic Therapy. *Mater. Sci. Eng. C* **2019**, *97*, 793–802. [CrossRef]
53. Jin, Q.; Liu, J.; Zhu, W.; Dong, Z.; Liu, Z.; Cheng, L. Albumin-Assisted Synthesis of Ultrasmall FeS2 Nanodots for Imaging-Guided Photothermal Enhanced Photodynamic Therapy. *ACS Appl. Mater. Interfaces* **2018**, *10*, 332–340. [CrossRef] [PubMed]
54. Li, Q.; Sun, L.; Hou, M.; Chen, Q.; Yang, R.; Zhang, L.; Xu, Z.; Kang, Y.; Xue, P. Phase-Change Material Packaged within Hollow Copper Sulfide Nanoparticles Carrying Doxorubicin and Chlorin E6 for Fluorescence-Guided Trimodal Therapy of Cancer. *ACS Appl. Mater. Interfaces* **2019**, *11*, 417–429. [CrossRef]
55. Liu, T.; Wang, C.; Cui, W.; Gong, H.; Liang, C.; Shi, X.; Li, Z.; Sun, B.; Liu, Z. Combined Photothermal and Photodynamic Therapy Delivered by PEGylated MoS2nanosheets. *Nanoscale* **2014**, *6*, 11219–11225. [CrossRef] [PubMed]
56. Sun, L.; Hou, M.; Zhang, L.; Qian, D.; Yang, Q.; Xu, Z.; Kang, Y.; Xue, P. PEGylated Mesoporous Bi2S3 Nanostars Loaded with Chlorin E6 and Doxorubicin for Fluorescence/CT Imaging-Guided Multimodal Therapy of Cancer. *Nanomed. Nanotechnol. Biol. Med.* **2019**, *17*, 1–12. [CrossRef]
57. Lu, K.; He, C.; Lin, W. A Chlorin-Based Nanoscale Metal-Organic Framework for Photodynamic Therapy of Colon Cancers. *J. Am. Chem. Soc.* **2015**, *137*, 7600–7603. [CrossRef] [PubMed]

58. Liu, C.; Luo, L.; Zeng, L.; Xing, J.; Xia, Y.; Sun, S.; Zhang, L.; Yu, Z.; Yao, J.; Yu, Z.; et al. Porous Gold Nanoshells on Functional NH2-MOFs: Facile Synthesis and Designable Platforms for Cancer Multiple Therapy. *Small* **2018**, *14*, 1–9. [CrossRef]
59. Halliwell, B.; Clement, M.V.; Long, L.H. Hydrogen Peroxide in the Human Body. *FEBS Lett.* **2000**, *486*, 10–13. [CrossRef]
60. Youssef, Z.; Jouan-Hureaux, V.; Colombeau, L.; Arnoux, P.; Moussaron, A.; Baros, F.; Toufaily, J.; Hamieh, T.; Roques-Carmes, T.; Frochot, C. Titania and Silica Nanoparticles Coupled to Chlorin E6 for Anti-Cancer Photodynamic Therapy. *Photodiagnosis Photodyn. Ther.* **2018**, *22*, 115–126. [CrossRef]
61. Xu, J.; Zhang, J.; Song, J.; Liu, Y.; Li, J.; Wang, X.; Tang, R. Construction of Multifunctional Mesoporous Silicon Nano-Drug Delivery System and Study of Dual Sensitization of Chemo-Photodynamic Therapy in Vitro and In Vivo. *J. Colloid Interface Sci.* **2022**, *628*, 271–285. [CrossRef]
62. Fan, J.; Qin, Y.; Xiao, C.; Yuan, L.; Long, Y.; Zhao, Y.; Nguyen, W.; Chen, S.; Chen, W.; Liu, X.; et al. Biomimetic PLGA-Based Nanocomplexes for Improved Tumor Penetration to Enhance Chemo-Photodynamic Therapy against Metastasis of TNBC. *Mater. Today Adv.* **2022**, *16*, 100289. [CrossRef]
63. Yin, Z.; Chen, D.; Zou, J.; Shao, J.; Tang, H.; Xu, H.; Si, W.; Dong, X. Tumor Microenvironment Responsive Oxygen-Self-Generating Nanoplatform for Dual-Imaging Guided Photodynamic and Photothermal Therapy. *ChemistrySelect* **2018**, *3*, 4366–4373. [CrossRef]
64. Ren, G.; Wang, Z.C.; Tian, Y.; Li, J.; Ma, Y.; Zhou, L.; Zhang, C.; Guo, L.; Diao, H.; Li, L.; et al. Targeted Chemo-Photodynamic Therapy toward Esophageal Cancer by GSH-Sensitive Theranostic Nanoplatform. *Biomed. Pharmacother.* **2022**, *153*. [CrossRef]
65. Liu, J.; Zhang, L.; Lei, J.; Shen, H.; Ju, H. Multifunctional Metal-Organic Framework Nanoprobe for Cathepsin B-Activated Cancer Cell Imaging and Chemo-Photodynamic Therapy. *ACS Appl. Mater. Interfaces* **2017**, *9*, 2150–2158. [CrossRef] [PubMed]
66. Lu, K.; He, C.; Guo, N.; Chan, C.; Ni, K.; Weichselbaum, R.R.; Lin, W. Chlorin-Based Nanoscale Metal-Organic Framework Systemically Rejects Colorectal Cancers via Synergistic Photodynamic Therapy and Checkpoint Blockade Immunotherapy. *J. Am. Chem. Soc.* **2016**, *138*, 12502–12510. [CrossRef]
67. Zheng, X.; Wang, L.; Liu, M.; Lei, P.; Liu, F.; Xie, Z. Nanoscale Mixed-Component Metal-Organic Frameworks with Photosensitizer Spatial-Arrangement-Dependent Photochemistry for Multimodal-Imaging-Guided Photothermal Therapy. *Chem. Mater.* **2018**, *30*, 6867–6876. [CrossRef]
68. Park, K.; Ahn, J.W.; Kim, J.H.; Kim, J.W. Tumor-Associated Macrophage-Targeted Photodynamic Cancer Therapy Using a Dextran Sulfate-Based Nano-Photosensitizer. *Int. J. Biol. Macromol.* **2022**, *218*, 384–393. [CrossRef] [PubMed]
69. Tan, P.; Cai, H.; Wei, Q.; Tang, X.; Zhang, Q.; Kopytynski, M.; Yang, J.; Yi, Y.; Zhang, H.; Gong, Q.; et al. Enhanced Chemo-Photodynamic Therapy of an Enzyme-Responsive Prodrug in Bladder Cancer Patient-Derived Xenograft Models. *Biomaterials* **2021**, *277*, 121061. [CrossRef] [PubMed]
70. Pantiushenko, I.V.; Rudakovskaya, P.G.; Starovoytova, A.V.; Mikhaylovskaya, A.A.; Abakumov, M.A.; Kaplan, M.A.; Tsygankov, A.A.; Majouga, A.G.; Grin, M.A.; Mironov, A.F. Development of Bacteriochlorophyll A-Based near-Infrared Photosensitizers Conjugated to Gold Nanoparticles for Photodynamic Therapy of Cancer. *Biochem. Mosc.* **2015**, *80*, 752–762. [CrossRef]
71. Zhang, K.; Yu, Z.; Meng, X.; Zhao, W.; Shi, Z.; Yang, Z.; Dong, H.; Zhang, X. A Bacteriochlorin-Based Metal–Organic Framework Nanosheet Superoxide Radical Generator for Photoacoustic Imaging-Guided Highly Efficient Photodynamic Therapy. *Adv. Sci.* **2019**, *6*, 1–9. [CrossRef]
72. Alsaab, H.O.; Alghamdi, M.S.; Alotaibi, A.S.; Alzhrani, R.; Alwuthaynani, F.; Althobaiti, Y.S.; Almalki, A.H.; Sau, S.; Iyer, A.K. Progress in Clinical Trials of Photodynamic Therapy for Solid Tumors and the Role of Nanomedicine. *Cancers* **2020**, *12*, 2793. [CrossRef] [PubMed]
73. Zhong, Y.T.; Cen, Y.; Xu, L.; Li, S.Y.; Cheng, H. Recent Progress in Carrier-Free Nanomedicine for Tumor Phototherapy. *Adv. Healthc. Mater.* **2022**, *2202307*, 1–32. [CrossRef] [PubMed]

Disclaimer/Publisher's Note: The statements, opinions and data contained in all publications are solely those of the individual author(s) and contributor(s) and not of MDPI and/or the editor(s). MDPI and/or the editor(s) disclaim responsibility for any injury to people or property resulting from any ideas, methods, instructions or products referred to in the content.